














Increased yield and CO₂ sequestration potential with the C₄ cereal *Sorghum bicolor* cultivated in basaltic rock dust-amended agricultural soil

Mike E. Kelland¹  | Peter W. Wade¹  | Amy L. Lewis¹  | Lyla L. Taylor¹  |
 Binoy Sarkar²  | M. Grace Andrews³ | Mark R. Lomas¹ | T. E. Anne Cotton¹  |
 Simon J. Kemp⁴  | Rachael H. James³  | Christopher R. Pearce⁵  | Sue E. Hartley¹  |
 Mark E. Hodson⁶  | Jonathan R. Leake¹  | Steven A. Banwart^{7,8}  | David J. Beerling¹ 

¹Leverhulme Centre for Climate Change Mitigation, Department of Animal and Plant Sciences, University of Sheffield, Sheffield, UK

²Lancaster Environment Centre, Lancaster University, Lancaster, UK

³School of Ocean and Earth Science, University of Southampton Waterfront Campus, Southampton, UK

⁴British Geological Survey, Environmental Science Centre, Nottingham, UK

⁵National Oceanography Centre, Southampton, UK

⁶Department of Environment and Geography, University of York, York, UK

⁷School of Earth and Environment, University of Leeds, Leeds, UK

⁸Global Food and Environment Institute, University of Leeds, Leeds, UK

Correspondence

David J. Beerling, Leverhulme Centre for Climate Change Mitigation, Department of Animal and Plant Sciences, The University of Sheffield, Sheffield S10 2TN, UK.
 Email: d.j.beerling@sheffield.ac.uk

Funding information

Leverhulme Trust, Grant/Award Number: RC-2015-029; NERC

Abstract

Land-based enhanced rock weathering (ERW) is a biogeochemical carbon dioxide removal (CDR) strategy aiming to accelerate natural geological processes of carbon sequestration through application of crushed silicate rocks, such as basalt, to croplands and forested landscapes. However, the efficacy of the approach when undertaken with basalt, and its potential co-benefits for agriculture, require experimental and field evaluation. Here we report that amending a UK clay-loam agricultural soil with a high loading (10 kg/m²) of relatively coarse-grained crushed basalt significantly increased the yield (21 ± 9.4%, SE) of the important C₄ cereal *Sorghum bicolor* under controlled environmental conditions, without accumulation of potentially toxic trace elements in the seeds. Yield increases resulted from the basalt treatment after 120 days without P- and K-fertilizer addition. Shoot silicon concentrations also increased significantly (26 ± 5.4%, SE), with potential benefits for crop resistance to biotic and abiotic stress. Elemental budgets indicate substantial release of base cations important for inorganic carbon removal and their accumulation mainly in the soil exchangeable pools. Geochemical reactive transport modelling, constrained by elemental budgets, indicated CO₂ sequestration rates of 2–4 t CO₂/ha, 1–5 years after a single application of basaltic rock dust, including via newly formed soil carbonate minerals whose long-term fate requires assessment through field trials. This represents an approximately fourfold increase in carbon capture compared to control plant–soil systems without basalt. Our results build support for ERW deployment as a CDR technique compatible with spreading basalt powder on acidic loamy soils common across millions of hectares of western European and North American agriculture.

KEYWORDS

carbon removal, crop productivity, mineral weathering, negative emissions technology, reactive transport modelling, silicon, soil acidification

This is an open access article under the terms of the Creative Commons Attribution License, which permits use, distribution and reproduction in any medium, provided the original work is properly cited.

© 2020 The Authors. *Global Change Biology* published by John Wiley & Sons Ltd

1 | INTRODUCTION

Deployment of large-scale carbon dioxide removal (CDR) strategies are required together with drastic phase-down of CO₂ emissions from fossil fuels to meet internationally agreed climate targets (UNEP, 2018). Research is therefore urgently required to determine efficacy, co-benefits, environmental risks, scalability and costs of such CDR strategies (EASAC, 2018; NRC, 2015; UNEP, 2018). Enhanced rock weathering (ERW) is a land-based CDR strategy addressing multiple UN Sustainable Development Goals (Smith et al., 2019) which involves amending agricultural soils with crushed abundant silicate rocks (e.g. basalt) to accelerate carbon capture. Implemented on croplands it has potential to increase production, protect against pests and diseases and assist in restoring acidified nutrient-depleted soils (Beerling et al., 2018; Hartmann et al., 2013; Kantola, Masters, Beerling, Long, & DeLucia, 2017; Zhang, Kang, Wang, & Zhu, 2018). The applied silicate minerals undergo reactions with CO₂ in the rhizosphere, releasing base cations (e.g., Ca²⁺, Mg²⁺) and alkalinity. Depending on soil chemistry, this can result in either the formation pedogenic carbonates or be delivered to the oceans via run-off; both routes store carbon with an estimated lifetime of tens of millennia (Hartmann et al., 2013; Renforth & Henderson, 2017). Minimizing adverse effects of ERW from mining, including associated impacts on biodiversity (Edwards et al., 2017) is contingent on exploiting existing silicate rock waste streams, for example, from quarries and legacy reserves, and artificial silicates (Beerling et al., 2018; Das, Kim, Hwang, Verma, & Kim, 2019; Manning, Renforth, Lopez-Capel, Robertson, & Ghazireh, 2013). Undertaken at large scale, ERW is a CDR strategy that may have potential to support food and soil security and help avert ocean acidification (Hartmann et al., 2013; Köhler, Hartmann, & Wolf-Gladrow, 2010; Taylor et al., 2016).

Numerical modelling investigations (Köhler et al., 2010; Taylor et al., 2016) have assessed the CDR potential of ERW largely in the context of tropical forests, but the focus is now turning towards croplands and soils on which deployment with existing land-spreading technology should be feasible (Beerling et al., 2018; Kantola et al., 2017; Strefler, Amann, Bauer, Kriegler, & Hartmann, 2018). Experimental and field trial programmes are thus underway examining CO₂ removal rates and feedbacks on crop performance and soil health. Such trials have reported rates of CO₂ removal following amendment of different agricultural soils across a range of application rates with the fast-weathering magnesium silicate, olivine (Amann et al., 2018; Dietzen, Harrison, & Michelsen-Correa, 2018; Renforth, Pogge von Strandmann, & Henderson, 2015; ten Berge et al., 2012). However, CO₂ removal by weathering of olivine-dominant dunite is often accompanied by increases in potentially toxic nickel (Ni) and chromium (Cr) concentrations that may be problematic for agricultural applications. Basalt rock is a proposed alternative silicate, containing at least six plant-essential nutrients (K, P, Ca, Mg, Fe and Mn) and very low concentrations of Cr and Ni (Beerling et al., 2018; Hartmann et al., 2013; Kantola et al., 2017). Although silicon (Si) is regarded as a non-essential

element for plants, cereals, the most important crops globally, accumulate Si in their straw and stover, with benefits for crop yield and resistance to abiotic and biotic stress (Debona, Rodrigues, & Datnoff, 2017; Guntzer, Keller, & Meunier, 2012). When crop residues are not returned to the land, this depletes the plant-available Si pools and can constrain yields (Haynes, 2017). Amending highly weathered soils of tropical agricultural regions with basalt increased yields of crops, and improved soil health (e.g. increased soil pH and cation exchange capacity [CEC]; Beerling et al., 2018; Edwards et al., 2017; Hartmann et al., 2013; Van Straaten, 2006). Additionally, soils produced from basaltic quarry fines have inorganic carbon sequestration potential via in situ carbonate formation, especially when mixed with organic matter (Manning et al., 2013). However, the amendment of soils with crushed basalt on crop production outside the tropics, possibly substituting in part for expensive rock-derived P- and K-fertilizers (Amann & Hartmann, 2019; Beerling et al., 2018), and its CDR potential remain to be assessed.

Here we investigate ERW carbon removal and co-benefits with the C₄ crop *Sorghum bicolor* grown at bench-scale in mildly acidic clay-loam agricultural soil amended with basaltic rock dust. *Sorghum* is one of the most widely cultivated cereal crops in the world and the fifth most important crop for food and animal feed, with the United States being the leading producer (Turhollow, Webb, & Downing, 2010). It also provides a representative functional type similar to the C₄ crop maize suitable for cultivation at the mesocosm scale under controlled environment conditions. *Sorghum* and maize are often grown in slightly acidic clay-loam soils that are important agricultural soils of western Europe and the United States. Depending on fertilizer treatment *Sorghum* can form symbiotic associations with arbuscular mycorrhizal (AM) fungi (Hindumathi & Reddy, 2011) that are important biotic agents of mineral dissolution (Quirk et al., 2012). Our experimental approach, therefore, is a first step towards understanding the potential applicability of ERW with basalt in a temperate-zone agricultural context which will be important for understanding suitability for large-scale deployment of this CDR strategy (Beerling et al., 2018; Haque, Santos, Dutta, Thimmanagari, & Chiang, 2019; Zhang et al., 2018). Basaltic mineral dissolution and carbon sequestration potential were assessed with elemental budgets (plants–soil–leachate pools). Over longer multiyear time horizons, we assess dissolution trajectories and resulting CDR using a 1 D reactive transport soil profile geochemical model calibrated to our experimental results, measured basalt mineralogy and particle size distribution.

2 | MATERIALS AND METHODS

2.1 | Weathering reactor design

Experiments were conducted with replicated mesocosms housed within the University of Sheffield controlled environment facility.

Weathering reactors were constructed from two lengths of 152 mm internal diameter polyvinyl chloride pipe, coupled by a polyurethane-sealed joint, where a 600 mm long upper-section contained the soil and a 400 mm long base-section housed the leachate collection assembly (Figure S1a). A 20 mm diameter nylon nozzle was set into the bottom of the soil-containing upper-section, to direct leachate into a 1 L amber Winchester bottle via a polytetrafluoroethylene funnel. A 50 mm deep drainage layer located at the base of the columns was used to prevent migration of soil particles into leachate nozzles, and comprised 5 mm diameter polyethylene beads placed on a high-density polyethylene screen (2 mm mesh size). Algal growth in the Winchester collection bottles, was minimized by enclosing them in detachable opaque plastic membranes. Column soil surfaces were dressed with a 50 mm deep polyethylene bead layer to reduce evaporation and minimize moss growth.

2.2 | Soil characterization and preparation

Mildly acidic soil (pH = 6.6; measurement protocol in Section 2.5) with a clay-loam texture (31.8%, 35.4% and 32.8% by mass of clay [$<2 \mu\text{m}$], silt [$2\text{--}60 \mu\text{m}$] and sand [$60\text{--}2,000 \mu\text{m}$], respectively) was collected from an agricultural field of *Brassica napus* (oil seed rape) at the Game and Wildlife Conservation Trust, Allerton Project, Leicestershire, United Kingdom (latitude 52.604328°N, longitude 0.825659°W). The soil had a CEC of 25.4 cmol (p^+)/kg, with >99% base saturation, and a low total organic carbon (TOC) content of 1.2% (wt%).

Prior to filling mesocosms, soil was manually comminuted by removing large stones and invertebrates, and then by passing through a rotary soil sieve (20 mm mesh size; model: CRS400, Clarke Power Products). A sub- and topsoil arrangement was engineered in the upper-section of the weathering reactor to simulate a tillage regime (Figure S1a), composed of 4.3 and 5.0 kg of soil, and compacted to an approximate bulk density of 1.05 and 1.2 kg/L respectively. The effective soil column length was 500 mm. Well-characterized crushed basalt (see Section 2.6; total mass of $181.5 \pm 0.5 \text{ g}$ per column; equivalent to 10 kg/m^2) from a typical volcanic arc mountain in the Cascade Range, Oregon, United States, was mixed with soil in the upper 250 mm of the treated columns ($n = 6$) to simulate plough layer mixing depth. This application rate is towards the upper limit of the practical range but lower than that used in a recent modelling study (15 kg/m^2 ; Strefler et al., 2018). Into this layer, we mixed a commercial AM fungal inoculum (25 g per column) to promote establishment of this symbiosis (PlantWorks UK Ltd). Planted weathering reactors containing only soil and mycorrhizal inoculum (without the basalt amendment) were maintained as the control treatment ($n = 6$). We also buried basalt-filled nylon mesh (35 μm diameter) bags (50 \times 50 mm) in the top 250 mm depth of the soil columns (2 per column) filled with 3 g of sieved and washed basalt grains (50–150 μm size fraction). The mesh was chosen to exclude roots but permit access to fungal hyphae from mycorrhiza. These bags were recovered at the end of the experiment to determine changes

in surface chemistry and analysis of the microorganisms colonizing the rock grains.

2.3 | Plant materials

Dwarf hybrid *S. bicolor* (Pennsylvania 115; Oakbank Game and Conservation) was cultivated in the weathering reactors. Approximately 300 seeds were pregerminated on filter paper (Whatman #1), moistened with distilled water, placed in zip-lock plastic bags and incubated at 25°C in darkness for 24 hr. About 100 seeds with roughly equal radicle length (ca. 5 mm) were selected for planting in seed-trays containing the experimental soil, transferred to the growth room, and maintained at 60%–70% relative humidity, with 18 hr/day at 25/17°C day/night temperatures. After 24 hr, 30 seedlings emerged from the soil, of which the 12 largest plants were grown for a further 14 days, before being randomly assigned for transplantation to weathering reactors in the growth room maintained under the same controlled environment conditions. Plants were grown under a photosynthetically active radiation (400–700 nm) of 800 $\mu\text{mol photons m}^{-2} \text{ s}^{-1}$, and for the first 60 days from emergence to boot stage, the day length was 18 hr but then shortened to 10 hr for the final 61 days until harvest. Plants were harvested at physiological maturity, segregated into root, shoot and seed parts, and dried in a forced-air oven at 60°C for 24 hr.

2.4 | Irrigation regime and effluent collection

Reactors were irrigated on a 5 day rotation basis using reverse osmosis water delivered via a bespoke drip-feed irrigation system at 12.5 ml/min (Figure S2, total irrigation amount of 13.9 L over 120 days). Urea was dissolved in irrigation water (total 0.71 g prilled urea per reactor during 120 day experiment) and supplied periodically to each reactor with the total addition rate representative of high yielding croplands worldwide (180 kg N/ha; Potter, Ramankutty, Bennett, & Donner, 2010). No P- or K-fertilizer was added during the experiment. Irrigation water supply was adjusted to produce about 150 ml of leachate about 24 hr after each irrigation event (Figure S2). Mean infiltration rate during the experiment was 2.1 mm/day. A 5% subsample of collected leachate was filtered through a Minisart 0.22 μm cellulose nitrate filter (Sartorius UK Ltd), and refrigerated at 4°C prior to chemical analyses.

2.5 | Leachate, soil, plant and rock analysis

Leachate and soil pH were measured with a Jenway 3540 Bench Combined Conductivity/pH Meter (Jenway). Measurements were standardized using a 3 point calibration on the hydrogen ion molar activity scale ($\text{pH} = -\log[\text{H}^+]$) using standard solutions at pH 4.00, 7.00 and 14.00. For soil pH measurements, 15 g of air-dried soil was

weighed into a 100 ml glass beaker and gradually mixed with 30 ml of deionized water (1:2 mass ratio of soil:water) using a glass stirrer, for 3 min. The solution was left to equilibrate with the atmosphere for 30 min before recording the measured pH of the slurry to 0.01 pH units. Dissolved cation concentrations in the leachate were quantified by Inductively Coupled Plasma Atomic Emission Spectrometry (ICP-AES; Spectro-Ciros-Vision, Spectro Analytical Instruments GmbH; detection limit for Mg/Ca/Sr = 0.001 mg/L; calibrated with multi-element standards from certified stock solutions). Soil exchangeable cations were isolated by leaching soil with 1 M ammonium acetate ($\text{NH}_4\text{CH}_3\text{CO}_2$; pH 7; Chapman, 1965), and subsequent elemental analysis of the extracts was conducted by ICP-AES. Soil and basalt total inorganic carbon (TIC) and TOC measurements were made using a CN Analyzer (Vario EL Cube; Elementar) on samples before and after treatment with 6 M HCl; soil: acid ratio of 90 mg to 0.5 ml ($n = 6$ homogenized samples per depth at four depths, 12.5, 25, 37.5 and 50 cm).

Sorghum root, shoot and seed masses were powdered separately using a grinding mill (Model: A10 S2; IKA-Werke GmbH & CO. KG). Cation concentrations were determined by digesting plant materials in 6 ml nitric acid and 2 ml perchloric acid mixture on a hot block (200°C) for 20 min and analysing the extracts by ICP-AES. Silicon concentrations in plant materials were measured following standard protocols (Reidinger, Ramsey, & Hartley, 2012) on pelletized powdered samples by X-ray fluorescence (XRF) spectroscopy (Spectros Niton XL3t900 GOLDD; Thermo Scientific) calibrated using Si-spiked synthetic methyl cellulose, and validated using Certified Reference Material NCS DC73349 'Bush branches and leaves' from the China National Analysis Center for Iron and Steel.

Basalt grains recovered from nylon bags were split into subsamples with one subjected to XRF spectroscopy measurements (Zetium; Malvern Panalytical Ltd) to determine changes in surface chemical element composition (Figure S3) and the others used for DNA extraction and subsequent molecular analysis to characterize the identity of microorganisms colonizing particles (Figure S4). Fungal colonization was examined by imaging the grains under a scanning electron microscope (SEM; VEGA3, TESCAN) at the Biomedical Sciences Electron Microscope Unit, University of Sheffield. Images were acquired using a secondary electron detector at an accelerating voltage of 20 kV under high vacuum conditions ($<1 \times 10^{-4}$ Torr; Figures S5 and S6, also see optical microscopy imaging in Figures S7 and S8).

DNA was extracted from basalt in the mesh bags using a DNeasy PowerSoil Kit (Qiagen Ltd). Amplification of partial 5.8S, ITS2 and partial 28S fungal sequences was performed by PCR with MyTaq™ Polymerase (Bioline) and primers gITS7 (Ihrmark et al., 2012) and ITS4 (White, Bruns, Lee, & Taylor, 1990), modified to include the Illumina overhang adapter sequences (Pétiacq et al., 2017). Triplicate PCRs were carried out on 1 µl of template DNA extract in the presence of the manufacturer's buffer (including dNTPs) and 0.4 µM of each primer in 20 µl reactions (PCR conditions: 94°C for 2 min; 35 cycles at 94°C for 30 s, 53°C for 30 s and 72°C for 30 s; and 72°C for 1 min). Products of the three PCR reactions were then pooled per sample

and purified using AMPure XP beads (Beckman Coulter Inc., USA). Dual indexes were added using the Nextera XT Index Kit (Illumina Inc. UK) following the manufacturer's instructions. Amplicons were then purified again using AMPure XP beads, quantified and pooled. Sequencing was performed using 250 bp sequencing on a MiSeq sequencer (Illumina Inc., at The Earlham Institute, Norwich, UK).

De-multiplexed FastQ files were filtered using USEARCH 9.1 (Edgar, 2010) with a maxEE value of 1. Only forward reads were analysed due to length variability in the ITS2 region producing potential biases for paired data. Primer sequences were removed and UCHIME was used to detect chimeras (Edgar, Haas, Clemente, Quince, & Knight, 2011). Comparisons were made to the QIIME/UNITE reference ITS database (v7.2; Nilsson et al., 2019) and sequences were clustered at 97% using QIIME (Caporaso et al., 2010). Singletons were removed from the data as these are often sequencing errors (Majaneva, Hyytiäinen, Varvio, Nagai, & Blomster, 2015). Sequences have been deposited in the European Nucleotide Archive under accession number PRJEB28082.

2.6 | Basaltic rock characterization

Pulverized basalt was sourced from the Cascade Mountain Range, Oregon (Central Oregon Basalt Products LLC). The rock is middle Miocene in age and belongs to the 'Prineville Chemical Type Unit' of the Columbia River Basalt (Smith & Hayman, 1987); with a chemical index of alteration of 38%, as calculated from the oxide data (Table S1; Nesbitt & Young, 1982), it is considered relatively unaltered. The mineralogy of the Oregon basalt (Table 1) was determined using X-ray diffraction (XRD) analysis at the British Geological Survey (BGS) Keyworth laboratories. Samples were spiked by 10% (wt%) with corundum (Al_2O_3) to aid quantitative analysis and spray-dried from an ethanol suspension at 80°C to ensure random orientation of mineral phases. Measurements were conducted on a PANalytical X'Pert-pro diffractometer (Malvern Panalytical Ltd.) using $\text{CoK}\alpha$ radiation ($\lambda = 1.78896 \text{ \AA}$) from 4.5–85° 2 θ run at 45 kV and 40 mA conditions. Crystalline mineral phases were identified using PANalytical HighScore Plus software coupled to the International Centre for Diffraction Data (ICDD) PDF-4+database. Crystalline mineral and amorphous material quantification was completed using the Rietveld refinement technique within the same HighScore Plus software package and using crystallographic information from the Inorganic Crystal Structure Database (Hellenbrandt, 2004) following the methodology in Kemp et al. (2016).

X-ray diffraction analysis indicated that the basalt contained a high percentage of amorphous material interpreted to be glass (~25%; Table 1). The elemental composition of the basaltic glass was determined with scanning electron microscopy-energy dispersive X-ray spectroscopy (SEM-EDX) to better constrain our reactive transport model (RTM) calculations (Figure S9; Table S2). Samples were carbon coated to approximately 25 nm thickness in an Agar AGB7367A automatic SEM carbon evaporation coater. Analysis was performed using a FEI QUANTA 600 SEM, operating at an

TABLE 1 Basalt mineralogy determined by X-ray diffraction and kinetic rate parameters (Palandri & Kharaka, 2004) used in the reactive transport modelling

Mineral name	Molecular formula	Weight	Acid kinetic parameters			Neutral kinetic parameters			Base kinetic parameters		
			logK	E _{app}	n	logK	E _{app}	logK	E _{app}	n	
Plagioclase ^a	Ca _{0.5} Na _{0.5} Al _{1.5} Si _{2.5} O ₈	35.1%	-7.87	42.1	0.626	-10.91	45.2	no data	no data	no data	
Alkali-feldspar ^b	K _{0.41} Na _{0.56} Ca _{0.03} Al _{1.03} Si _{2.97} O ₈	23.0%	-10.06	51.7	0.5	-12.41	38	-21.2	94.1	-0.82	
Diopside (Mang)	Ca _{0.87} Mg _{0.94} Mn _{0.19} Si ₂ O ₆	6.2%	-6.36	96.1	0.71	-11.11	40.6	no data	no data	no data	
Diopside	CaMg _{0.7} Al _{0.6} Si _{1.7} O ₆	4.4%	-6.36	96.1	0.71	-11.11	40.6	no data	no data	no data	
Apatite	Ca ₃ (PO ₄) ₃ (OH)	2.8%	-4.29	250	0.171	-6	250	no data	no data	no data	
Montmorillonite	Ca _{0.6} Al ₂ Si ₄ O ₁₀ (OH) ₂ ·H ₂ O	1.2%	-12.71	48	0.22	-14.41	48	-14.41	48	-0.13	
Olivine ^c	Fe _{0.9%} Mg _{1.04} SiO ₄	1.0%	-6.85	67.2	0.47	-10.64	79	no data	no data	no data	
Ilmenite	Fe _{1.4} Ti _{0.6} O ₃	0.6%	-8.35	37.9	0.421	-11.16	37.9	no data	no data	no data	
Quartz	SiO ₂	<0.5%	-9.98	87.7	0.31	-13.99	87.7	-14.96	87.7	-0.41	
Basaltic glass ^d	Na _{0.13} Ca _{0.08} Mg _{0.05} K _{0.10} Fe _{0.12} Al _{0.26} SiO _{2.86}	24.9%									
Calcium carbonate ^e	CaCO ₃	0.34 ± 0.07%									

Note: Weathering rates for each mineral were modelled using the following equation (Palandri & Kharaka, 2004):

$$\frac{dm}{dt} = -SA \left[k_{\text{acid}}^{298.15\text{K}} e^{-\frac{E_{\text{acid}}}{R} \left(\frac{1}{T} - \frac{1}{298.15} \right)} a_{\text{H}^+}^{n_1} (1 - \Omega)^{q_1} + k_{\text{neut}}^{298.15\text{K}} e^{-\frac{E_{\text{neut}}}{R} \left(\frac{1}{T} - \frac{1}{298.15} \right)} (1 - \Omega)^{q_2} + k_{\text{base}}^{298.15\text{K}} e^{-\frac{E_{\text{base}}}{R} \left(\frac{1}{T} - \frac{1}{298.15} \right)} a_{\text{H}^+}^{n_3} (1 - \Omega)^{q_3} \right],$$

where $\frac{dm}{dt}$ is the weathering rate, SA is the mineral surface area, $k_i^{298.15\text{K}}$ is the dissolution rate constant for the respective mechanisms at 298.15 K, E_i is the apparent activation energy, R is the gas constant, T is the temperature in K, a_{H^+} is the hydrogen ion activity, n_i is the order of the reaction, Ω is the mineral saturation index and p_i and q_i are dimensionless empirical constants for the particular mineral.

^aRate constant is for labradorite (the plagioclase mineral closest to the XRD-derived stoichiometry).

^bRate constant taken for albite and for K-feldspar (substituting for sanidine).

^cModelled as iron-rich forsterite.

^dStoichiometry derived from SEM/EDX analysis of basalt amorphous material (Table S2). Basaltic glass dissolution rates modelled using the following equation (Gislason & Oelkers, 2003):

$$r_{+,\text{geo}} = A_A \exp\left(-\frac{E_A}{RT}\right) \left(\frac{a_{\text{H}^+}^3}{a_{\text{Al}^{3+}}} \right)^{1/3},$$

where $r_{+,\text{geo}}$ is the geometric surface area-normalized steady-state basaltic glass dissolution rate, A_A is a constant equivalent to $10^{-5.6}$ (mol of Si) $\text{cm}^{-2} \text{s}^{-1}$, E_A is a pH-independent activation energy of 25.5 kJ/mol, R is the gas constant, T is the temperature in K, and a_i is the activity of the respective aqueous species.

^eWeight derived from carbon analysis of unweathered basalt samples using a CN Analyser, before and after treatment with 6 M HCl. Calcium carbonate in basalt was modelled as an equilibrium phase.

accelerating voltage of 20 kV, spot size 5 and under high vacuum conditions ($<1 \times 10^{-4}$ Torr) also at the BGS laboratories. Energy dispersive X-ray analysis was conducted using Oxford Instruments X-MAX large area (50 mm²) silicon drift detector, running with Oxford Instruments INCA (v4) software. The EDX system was used to identify the point-elemental compositions from samples and is capable of detecting elements from atomic number 4 (B) to atomic number 92 (U) with a detection limit of the order of 0.2–0.5 weight % for most elements. Areas of the amorphous glassy phase were identified from backscattered electron images and relevant spectra and concentration determined from point analyses.

Bulk pulverized basalt was split into representative samples using a spinning riffler (Microscal), and the particle size distribution was established using a laser diffraction particle size distribution analyzer (Model: LA-950; Horiba UK Ltd). The p80 value (80% of the particles have a diameter less than or equal) of the soil-applied pulverized basalt was 1,250 μm (Figures S10 and S11). Specific surface area measurements were made using the Brunauer–Emmett–Teller (BET) N₂-adsorption (Brunauer, Emmett, & Teller, 1938) method using a Micromeritics Gemini VII 2390a instrument (Micromeritics Instrument Corporation; Figure S12; Table S3).

2.7 | Sr isotope analyses

Radiogenic Sr isotope (⁸⁷Sr/⁸⁶Sr) analyses were conducted in the clean laboratory facilities at the University of Southampton. Leachate samples for radiogenic Sr isotope measurements were acidified to pH < 2 using concentrated HNO₃. *Sorghum* shoot samples for radiogenic Sr isotope measurements were digested with 5 ml of concentrated nitric acid in a microwave digestion system, dried, reacted with 30% H₂O₂ to ensure complete oxidization of organic compounds, dried, redissolved in 3% HNO₃, and finally passed through 0.45 μm polypropylene syringe filters (Whatman Puradisc). To isolate exchangeable soil cations for radiogenic Sr isotope measurements, 1.0 g soil subsamples were reacted with 1 M NH₄Cl adjusted to pH = 8 for 24 hr and then centrifuged. The supernatants were passed through 0.45 μm polypropylene syringe filters (Whatman Puradisc), dried and redissolved in 3% HNO₃. A 10 g subsample of the basalt rock was powdered in a shatterbox. The carbonate and silicate fractions of the powdered rock were isolated using a sequential leaching and digestion procedure. To isolate the carbonate fraction, subsamples of the powder (~1.0 g) were reacted with 4 M acetic acid for 24 hr. The mixtures were centrifuged, and the supernatants were passed through 0.45 μm polypropylene syringe filters (Whatman Puradisc) and collected in Teflon beakers. Filtered supernatants were dried and redissolved in 3% HNO₃. The remaining residues, assumed to represent the silicate fraction, were oven dried, and 0.1 g subsamples were reacted in a 5:3 mixture of concentrated HF and HNO₃ at 140°C, dried, refluxed in concentrated HNO₃, dried, refluxed in 6 N HCl, dried and finally, redissolved in 3% HNO₃. Sr concentrations of all samples (water, plant, soil, rock) were measured on a Thermo-Fisher iCAP 6500 Inductively Coupled Optical

Emission Spectrometer (ICP-OES) at the National Oceanography Centre Southampton (Table S4). Sr concentrations were within $\pm 5\%$ of reported values for standards analysed throughout the analyses.

Radiogenic Sr isotope measurements were conducted using a Thermo-Scientific Triton Thermal Ionization Mass Spectrometer (TIMS) following methods presented in Andrews, Jacobson, Lehn, Horton, and Craw (2016). Briefly, sample aliquots containing 200 ng of Sr were dried, redissolved in 8 M HNO₃, and eluted through inverted pipette tips packed with Sr-Spec resin. The purified Sr fractions were dried, redissolved in 2 μl of 8 N HNO₃, and loaded onto single, outgassed Re filaments with 1 μl of a TaCl₅ solution. Ion beams were collected in multidynamic mode. To correct for instrumental mass fractionation, the ⁸⁶Sr/⁸⁸Sr ratio was normalized to 0.1194 using an exponential law. During analysis of ⁸⁷Sr/⁸⁶Sr ratios, the ⁸⁵Rb ion beam was monitored to ensure that ⁸⁷Rb did not isobarically interfere with ⁸⁷Sr. No interferences were observed. For the period of study, repeated analyses of NBS 987 standard yielded a mean ⁸⁷Sr/⁸⁶Sr ratio of 0.710250 ± 0.000008 ($\pm 2\sigma\text{SD}$, $n = 6$). The current long-term, mean ⁸⁷Sr/⁸⁶Sr ratio is 0.710251 ± 0.000010 ($\pm 2\sigma\text{SD}$, $n = 32$).

For treatment samples, we used a two-component isotope mixing equation to determine the mole fraction of Sr in cation reservoirs derived from basalt weathering (f_x), as opposed to soil weathering:

$$f_x = \frac{\delta_x - \delta_{\text{soil}}}{\delta_{\text{basalt}} - \delta_{\text{soil}}}, \quad (1)$$

where δ denotes the ⁸⁷Sr/⁸⁶Sr ratio of the treatment cation reservoir ($x = \text{plant, exchangeable soil, or leachate}$), the corresponding control cation reservoir ('soil') and the basalt silicate digest or basalt carbonate leachate ('basalt').

2.8 | Reactive transport model

Column reactors were conceptualized as a 250 mm deep soil column constituting five 50 mm deep cells, and a 50 mm deep well-mixed fluid reservoir in contact with the atmosphere at the base of the column. The RTM was constructed with the PHREEQC platform (Parkhurst & Apello, 2013) using the T&H.dat geochemical reaction database (Apello & Postma, 2005), which includes surface complexation constants for particulate organic matter based on the WHAM model (Tipping, 1998; Tipping & Hurley, 1992). Speciation of oxidized and reduced forms of nitrogen was explicitly decoupled to allow for irreversible kinetic transformations of excess urea fertilizer to nitrate, as observed empirically. Flow of irrigation water through the column was simulated by a time series of irrigation events at the top of the soil that resulted in 1 D vertical flow of pore solution and advection of solutes through the layers producing the overall mass of leachate from the columns (4.58 L in 120 days). The model incorporated chemical dissolution of source minerals having the measured stoichiometries of basaltic mineral phases, and their relative mass concentrations, as identified by the XRD results (Table 1).

Reactive surface area for each mineral was apportioned according to the mineral weight per cent of the basalt grains.

Chemical dissolution rate laws and coefficients for basaltic glass were sourced from Flaathen, Gislason, and Oelkers (2010) and those for other minerals from the US Geological Survey (Palandri & Kharaka, 2004). Solubility constants of the basaltic minerals were taken from the THERMODDEM database (Blanc et al., 2012) and for the basaltic glass from Aradóttir, Sonnenthal, and Jónsson (2012). Changes in reacting particle sizes due to element mass transfer to solution during dissolution were simulated using the shrinking particle model (Rimstidt, 2014). Background weathering of soil minerals was represented by a porewater solution chemically identical to leachate from the basalt-free systems. Figures S13 and S14 provide schematic and systems diagrams, respectively, defining the process and interactions of the RTM.

Modelled geochemical processes included equilibrium of dissolved inorganic carbon species with atmospheric CO_2 , and a profile of partial pressures of CO_2 in the soil profile representing autotrophic and heterotrophic respiration (Nan, Yue, Li, Huang, & Shen, 2016). Apparent reactive surface area (RSA) and CEC were optimized within MATLAB (version 2019a; The MathWorks, Inc.) using the 'fmincon' function. Separate optimizations were performed on individual treated columns with several candidate sinks for Al and Fe (amorphous $\text{Al}(\text{OH})_3$ and $\text{Fe}(\text{OH})_3$, gibbsite, kaolinite, and goethite). Based on the smallest root-mean-square errors between model and observed leachate Al (Figures S15 and S16) and 18 leachate and extractable elements (Figures S17 and S18), our solid equilibrium phases are determined to be amorphous $\text{Al}(\text{OH})_3$ and $\text{Fe}(\text{OH})_3$, along with calcite, amorphous silica and pyrophyllite (MnO_2). These phases react reversibly on the relatively short residence times of the soil fluids. We optimized apparent CEC because measured CEC will include the charge separately represented by the WHAM model, and because our single extraction method could have resulted in dissolution of existing phases, such as calcite. Our optimizations suggest less than $10 \text{ cmol}_c/\text{kg}$ soil of the total observed charge is unaccounted for in our model (Figure S19).

Cation exchange on clay surfaces was modelled using the default exchange convention in the PHREEQC code. Exchange site composition was initially determined by equilibration with the measured ionic composition of soil pore waters in the basalt-free control experiments with optimized CEC. The total number of sorption sites attributable to organic matter was derived from the concentration of extractable organic matter, as determined experimentally. Following the protocol described in Example 19 of the PHREEQC documentation (Parkhurst & Apello, 2013), these sites were apportioned to the 20 WHAM surface species using WHAM constant charges of -1.42 meq/g humic acid for four monoprotic phenolic sites, -2.84 meq/g humic acid for all diprotic or carboxylic sites and total charge -7.1 meq/g humic acid. CO_2 capture was calculated as the sum of HCO_3^- exported in leachate plus CO_2 incorporated into pedogenic carbonate minerals minus half of the HCO_3^- originating from weathering of carbonate mineral component of the basalt (Table 1).

In the model, growth of *Sorghum* influences the geochemistry of the system by removing Ca, Mg and Si from the soil with concomitant release of hydrogen ions to the soil. Using an average leachate chemistry from our control columns as our influent, implicitly accounts for both dissolution of existing soil minerals and 'background' plant growth unrelated to the treatment. *Sorghum* growth due to the treatment is therefore the difference between growth in the individual treated column and the average growth in control columns. *Sorghum* growth was modelled as a linear function which removed ions at a constant rate up to the maximum plant growth at 120 days, when harvesting of the plant was simulated by switching off the growth function for the rest of the annual cycle. In the 5 year modelling scenarios, a new growth cycle was modelled, as described above, for the first 120 days of each year, followed by a fallow period until the beginning of the next year.

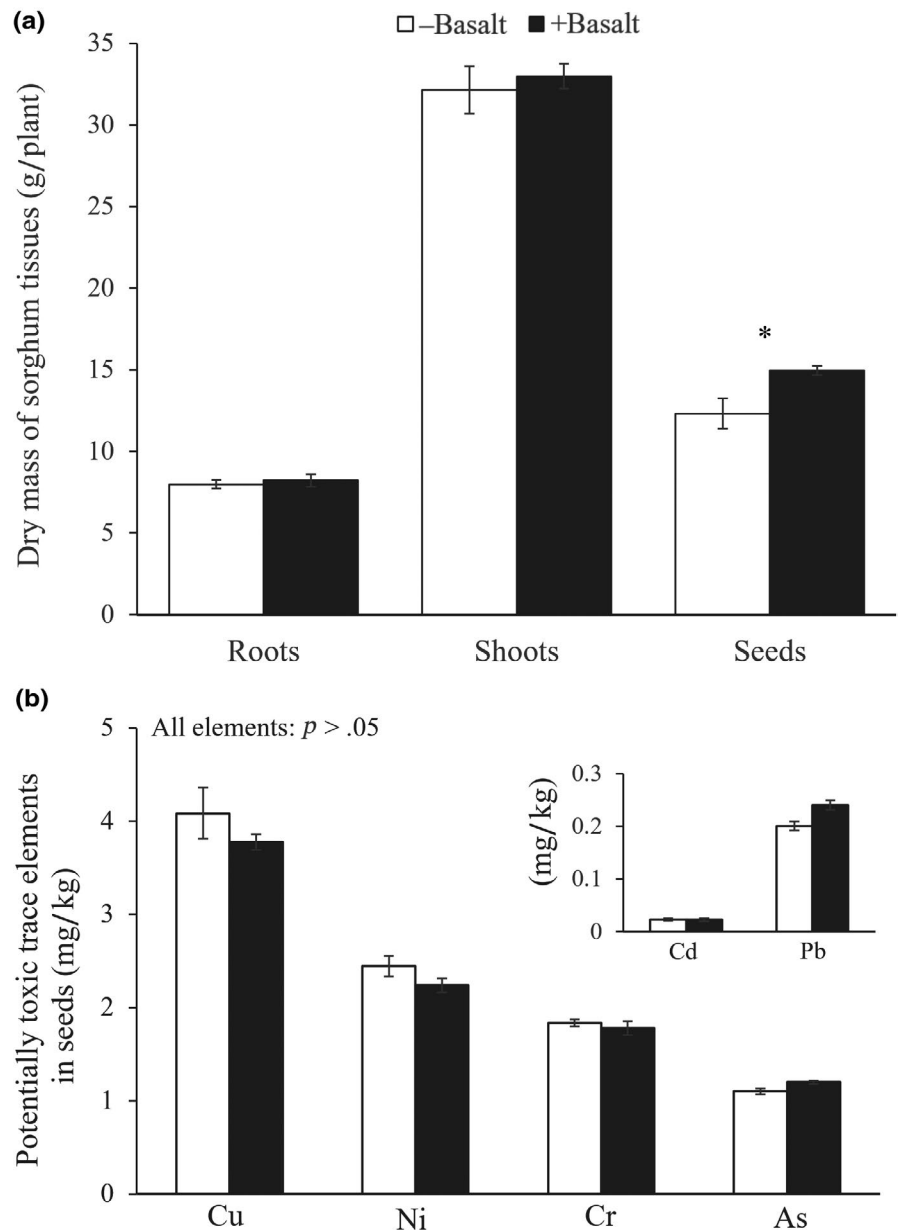
3 | RESULTS AND DISCUSSION

3.1 | *Sorghum* yield response

After 120 days, yield of mature *Sorghum*, measured as seed dry mass per plant, increased significantly by $21 \pm 9.4\%$ (SE) in response to the basalt treatment compared to control plants ($p < .05$, ANOVA) with no significant changes in shoot or root biomass (Figure 1a). Yield improvements occurred without significantly ($p > .05$) increased seed concentrations of potentially toxic trace elements from basalt (Figure 1b). The yield increase in *Sorghum* occurred without addition of P and K fertilizer and is comparable to that reported for the C_4 crop sugarcane in field trials with crushed basalt applications of $1\text{--}10 \text{ kg/m}^2$, in combination with standard N-P-K fertilizer treatments, on the highly weathered soils of Mauritius (de Villiers, 1961). Over five successive harvests in that study, sugarcane yields increased by up to 30% compared with plots receiving fertilizer and no basalt addition (de Villiers, 1961).

The average 21% increase in *Sorghum* yield we report (Figure 1a) is comparable with the biomass increase of perennial ryegrass (15.6%) following amendment of an acidic ($\text{pH} = 4.9$) sandy soil with olivine in controlled environment experiments ($0.16\text{--}20.4 \text{ kg/m}^2$) but which resulted in the accumulation of Ni in soils (ten Berge et al., 2012). Haque et al. (2019), however, reported substantially higher increases in the biomass of the C_4 crop *Zea mays* L. and the N_2 -fixing legume *Phaseolus vulgaris* L. (90% and 177%, respectively), following additions of wollastonite (221 t/ha) to an acidic ($\text{pH} = 4.9$) agricultural soil. If replicated under field conditions, our results suggest incorporating crushed basalt into agricultural land management practices could reduce demand for expensive conventional rock-derived fertilizers (P, K and Ca; Amann & Hartmann, 2019; Beerling et al., 2018) and agricultural lime, with increasing yields improving profit margins for farmers. Such effects could lower barriers to future deployment of ERW as a CDR strategy by offsetting the costs (Amann & Hartmann, 2019; Beerling et al., 2018).

FIGURE 1 Effect of basalt-amended soil on yield and chemistry of *Sorghum* biomass. (a) Root, shoot and seed dry mass, (b and inset) concentrations of potentially toxic trace elements in seeds. Error bars represent SE ($n = 6$ columns per treatment). The asterisk denotes that the result is statistically significant at the 5% level (i.e. $p < .05$)



3.2 | Elemental budgets of *Sorghum* plants

Plant elemental budgets showed significant increases in whole plant Si ($p < .05$), Ca and Sr pools ($p < .01$; Figure 2a,b,f), with overall Mg, K and P budgets remaining unchanged, but seed K increasing significantly ($p < .05$; Figure 2c–e). Crushed basalt provided the only supplemental source of Si, Ca, K and Sr, and uptake and accumulation of these elements in *Sorghum* shoots, allied to increases in soil pH (see below), indicates mass transfer from the source rock on the timescale of the experiment. Increased shoot Si can enhance the resilience of plants to abiotic stresses, including drought, salinity, heat (Burghelea et al., 2015; Korchagin, Caner, & Bortoluzzi, 2019) and resistance to lodging due to wind or rain (Artyszak, 2018) as well as to biotic attack (Meharg & Meharg, 2015; Van Bockhaven, De Vleeschauwer, & Höfte, 2012).

Shoot Si increases following soil silicate treatments, for example, provided direct protection from pests and diseases for major C_3 (soybean, wheat and rice) and C_4 crops (sugarcane and maize) and indirect protection via changes in the release of herbivore-induced plant volatiles enhancing parasitoid attraction (Liu et al., 2017).

Significantly increased total shoot Si mass ($26 \pm 5.4\%$, SE) following basalt treatment in our experiment mirrors increased concentrations of Si in rye grass biomass following addition of olivine (Si, 50%–180% increase; ten Berge et al., 2012). However, in these experiments, olivine significantly increased Mg and reduced plant Ca uptake by 7%–58% compared to results with basalt in our study: increases of $11 \pm 3.1\%$ (SE) in Ca and $11 \pm 2.5\%$ (SE) in its geochemically similar tracer Sr, but no change in plant Mg uptake (Figure 2b,e,f).

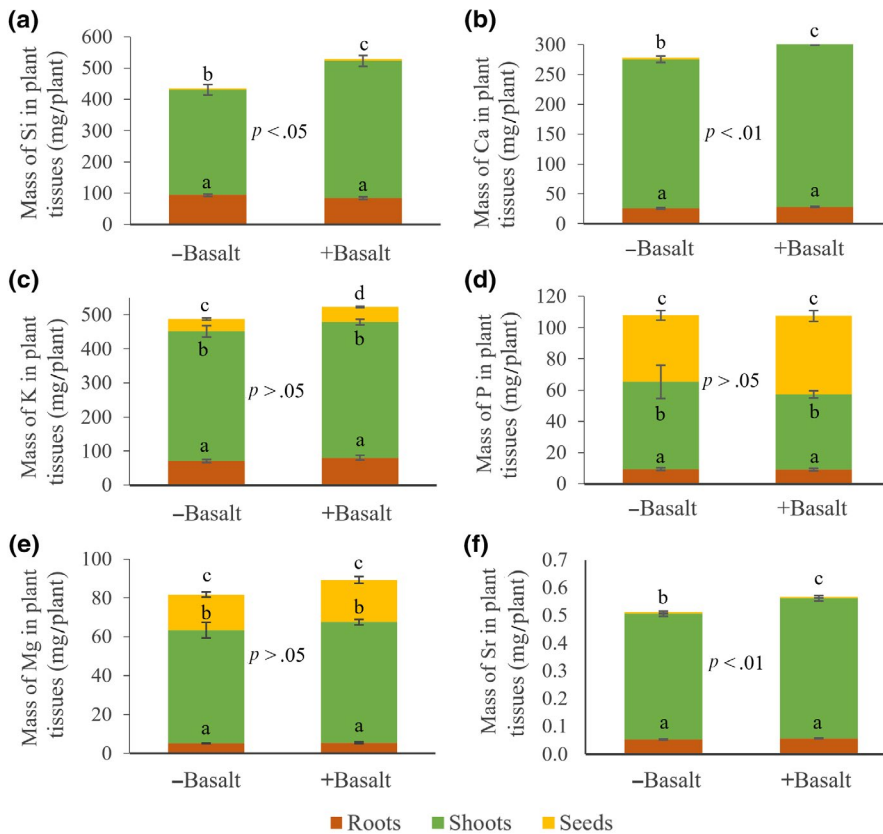


FIGURE 2 Effect of basalt-amended soil on *Sorghum* tissue elemental budgets. (a) Silicon, (b) calcium, (c) potassium, (d) phosphorus, (e) magnesium and (f) strontium. Bars sharing the same letter are not statistically different ($p > .05$). Error bars represent standard errors ($n = 6$ columns per treatment)

3.3 | Leachate and soil biogeochemistry

Increased leachate pH (Figure 3a) is consistent with basalt weathering; calcium-silicate mineral dissolution consumes hydrogen ions and produces alkalinity. Similar pH increases followed basalt amendment of acidic weathered tropical soils and reduced Al toxicity, a factor limiting plant growth on acidic soils (Anda, Shamshuddin, & Fauziah, 2013, 2015; Gillman, 1980). Mitigation of soil acidification by basaltic rock dust weathering indicates its potential to substitute for the practice of liming. This could avert CO₂ emissions during production and application of lime to soils; in the United States alone this has been estimated to contribute 2% of agricultural greenhouse gas emissions (West & McBride, 2005). For comparison, application of 20.4 kg/m² of olivine to an acidic sandy soil increased the pH from 4.8 to 6.0 after 224 days, but also increased the uptake of Ni originating from the olivine in ryegrass (ten Berge et al., 2012).

Ammonium acetate extractable soil Si, and the exchangeable pool of soil Mg increased significantly ($p < .01$, ANOVA) in response to the basalt treatment, although there was no significant effect on exchangeable Ca (Figure 3f-h). Marked increases in soil exchangeable pools of Mg (200%–700%) occurred in planted olivine mesocosm weathering trials (Amann et al., 2018; ten Berge et al., 2012). Replenishment of depleted soluble Si pools by basalt weathering as seen in the present work represents a substantial co-benefit of ERW because repeated biomass harvesting of silica accumulating crops by intensive cultivation depletes plant-available Si in soils (Haynes, 2017). Crop production and harvesting in the United States, for

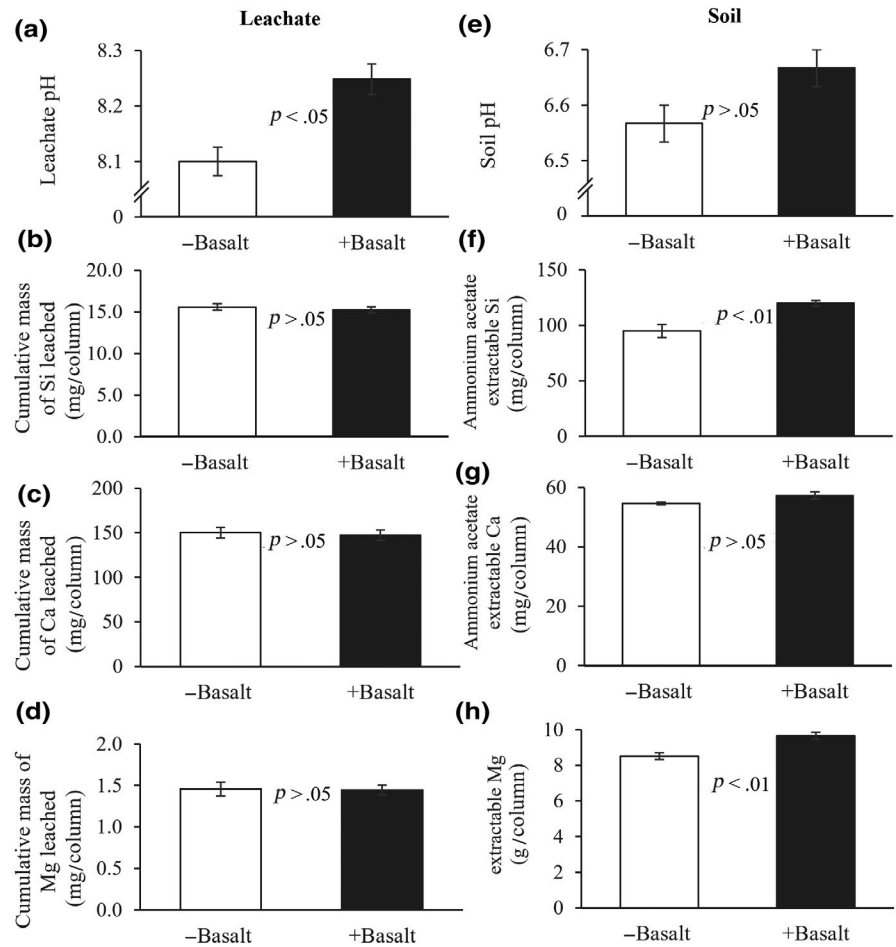
example, removes an estimated 19 million tonnes of silica annually and negatively affects yields, especially of sugarcane and rice (Tubana, Babu, & Datnoff, 2016). Adoption of Si-fertilization practices, such as dressing soils with natural and artificial silicates, to maintain crop yields could help redress the problem in Europe and North America (Artyszak, 2018; Crooks & Prentice, 2017), and the tropics (Ma, 2004; Ma & Yamaji, 2006; Meena et al., 2014). In east Asia, this approach has been practiced for the past decade to improve crop production (Cuong, Ullah, Datta, & Hanh, 2017; Li et al., 2018).

We detected no significant changes in leachate Si, Mg or Ca following the basalt treatment after 120 days (Figure 3b-d), suggesting elements released by weathering were retained in the plant-soil system in this study. Lack of leachate chemistry response has also been observed following a very high olivine application (220 t/ha) to loamy soils (pH = 7.8) supporting the growth of wheat and barley (Amann et al., 2018). We also found no statistical change ($p > .05$) in alkalinity between treatments as determined by charge balance ($1,148 \pm 245 \mu\text{eq/L}$ [1 SD, $n = 6$] without basalt vs. $1,100 \pm 147 \mu\text{eq/L}$ [1 SD, $n = 6$] with basalt); these values are within the range of agricultural sites (350–3,800 $\mu\text{eq/L}$; Fortner et al., 2012).

3.4 | Element release from basalt weathering

Comparison of the total measured amount of Ca, Mg and Si in the exchangeable soil cations, column leachate and plant tissues (biomass [Figure 1a] \times concentration [Figure S20]) provides a minimum

FIGURE 3 Effect of basalt-amended soil on leachate and soil chemistry. (a) Soil pH, (b) soil exchangeable silica, (c) calcium and (d) magnesium concentrations. (e) Leachate pH, and cumulative mass of (f) silicon, (g) calcium and (h) magnesium leached through the soil columns with and without the basalt treatment. Error bars represent standard errors ($n = 6$ columns per treatment)



estimate of mass transfer of these elements from basalt weathering into the plant–soil system (Table 2). Additional mass transfer resulting in formation of secondary minerals is not accounted for in these sampling procedures but may be inferred from geochemical modelling. Measured major cationic elements released by basaltic grain weathering were generally retained in the soil exchange pool (Table 2; as confirmed in Section 3.5). The ultimate fate of these accumulated base cations is important for carbon capture but is uncertain. If flushed from the soil profile into run-off over time, they constitute a weathering flux per m^2 of land area, as typically measured by dissolved element fluxes represented by base cations ($2Ca^{2+} + 2Mg^{2+} + Na^+ + K^+$, eq/m^2 land $time^{-1}$) in streamwater draining from watersheds that plays a key role in CO_2 removal.

Calculated element mass transfer rates ($mol\ m^{-2}\ s^{-1}$) from dissolving basalt grains on a per unit physical surface area of rock (based on BET surface area; $7.35\ m^2/g$), using elemental budgets in the plant, soil and leachate pools, yields dissolution rates that can be compared with literature values. We also calculate dissolution rates based on measured Mg released. Mg is present in the most reactive components of our basalt (olivine and diopside; Table 1) and is less affected by plant uptake (Figure 2) and secondary mineral precipitation than Ca. This is consistent with significant ($p < .05$) Mg depletion on the grain surfaces, as determined by XRF (Figure S3). We have not used dissolved Si as a tracer for mineral

dissolution due to potential retention as amorphous silicate coatings that have not been quantified, for example, on soil and basalt particles (Daval et al., 2011). Rates for Mg release normalized to the BET surface area of our milled basalt rock ($10^{-13}\ mol\ m^{-2}\ s^{-1}$; Table 2) are a similar order of magnitude to those observed for dissolving Mg-rich olivine mineral grains in planted mesocosm experiments ($10^{-13.1}$ – $10^{-13.7}\ mol\ m^{-2}\ s^{-1}$; Amann et al., 2018; $10^{-11.8}$ – $10^{-12.7}\ mol\ m^{-2}\ s^{-1}$; Renforth et al., 2015). The mineralogy of the basalt (Table 1) suggests that if Mg were being released primarily from the olivine exposed at the surfaces of the grains, the release rate normalized to olivine surface area would give a calculated rate approximately 100-fold higher. This assumes that olivine surface area as a fraction of measured surface area scales with wt% olivine in the basalt. These much higher Mg mass transfer rates are similar to those reported in the literature for olivine dissolution in laboratory weathering experiments. Rates reported by Amann et al. (2018) in planted mesocosms were based on dissolved Mg flux in leachate only and did not account for accumulation on soil ion exchange surfaces, such as clay minerals. In our study, this exchangeable pool accumulated a 100-fold excess or more of released cations compared to the plant and leachate pools of released Mg (Table 2).

The BET method is postulated to overestimate RSA of dissolving minerals due, in part, to measuring internal pore surface area

TABLE 2 Changes in whole-system elemental budgets and transfer rates resulting from soil amendment with basalt after 120 days. Values are mean differences between basalt-amended ($n = 6$) and unamended (control) planted reactor columns ($n = 6$). Positive values indicate increased element concentrations due to basalt amendments. Soil extraction results are averages (\pm SE) for subsamples taken from six equidistant depths. Surface areas are expressed as SA_L for land surface area, and SA_R for rock surface area

Effect of basalt treatment on rate of elemental release							
Element	Leachate			Plant		Rate of elemental release (SSA = $7.35 \text{ m}^{-2} \text{ g}^{-1} \text{ basalt}^c$) ($\text{mol m}^{-2} \text{ SA}_R \text{ s}^{-1}$)	
	$(\mu\text{mol m}^{-2} \text{ SA}_L \text{ day}^{-1})$	Roots	Shoots	Seeds	Soil extraction ^a ($\text{mmol m}^{-2} \text{ SA}_L \text{ day}^{-1}$)		Measured elemental release from basalt ^b ($\text{mmol m}^{-2} \text{ SA}_L \text{ day}^{-1}$)
Ca	-31 ± 91	26 ± 22	300 ± 84	1.9 ± 2.7	17 ± 14	18 ± 14	$2.8 \times 10^{-12} \pm 2.2 \times 10^{-12}$
Mg	-0.35 ± 5.1	5.5 ± 7.4	72 ± 79	63 ± 40	4.0 ± 0.91	4.2 ± 0.93	$6.6 \times 10^{-13} \pm 1.5 \times 10^{-13}$
K	30 ± 17	110 ± 96	210 ± 210	96 ± 44	0.68 ± 1.3	1.1 ± 1.4	$1.8 \times 10^{-13} \pm 2.3 \times 10^{-13}$
Na	-0.63 ± 11	0.52 ± 3.7	4.2 ± 5.0	0.3 ± 1.3	0.33 ± 0.53	0.33 ± 0.53	$5.2 \times 10^{-14} \pm 8.4 \times 10^{-14}$
Si	-5.2 ± 8.5	-140 ± 90	$1,600 \pm 390$	1.7 ± 1.5	0.36 ± 0.10	1.9 ± 0.4	$2.9 \times 10^{-13} \pm 6.9 \times 10^{-14}$

^aDerived from ammonium acetate extraction on soil samples representative of the whole column.

^bMeasured moles released from basalt, Q, is calculated:

$$Q = A_{\text{Bas}} + B_{\text{Bas}} + C_{\text{Bas}} + D_{\text{Bas}} + E_{\text{Bas}} - (A_{\text{Con}} + B_{\text{Con}} + C_{\text{Con}} + D_{\text{Con}} + E_{\text{Con}}),$$

where A, B, C, D and E are the measured moles of the element in the leachate, roots, shoots, seeds and soil extraction, and the subscripts Bas and Con relate to the basalt treatment and control. The overall uncertainty, δQ , is calculated by summing the errors for each system component in quadrature, using the following equation (Kirchner, 2001),

$$\delta Q = \sqrt{\delta A_{\text{Bas}}^2 + \delta B_{\text{Bas}}^2 + \delta C_{\text{Bas}}^2 + \delta D_{\text{Bas}}^2 + \delta E_{\text{Bas}}^2 + \delta A_{\text{Con}}^2 + \delta B_{\text{Con}}^2 + \delta C_{\text{Con}}^2 + \delta D_{\text{Con}}^2 + \delta E_{\text{Con}}^2}$$

^cCalculated by dividing the measured moles released from basalt by BET-determined rock surface area (SSA = $7.35 \text{ m}^2/\text{g}$ basalt).

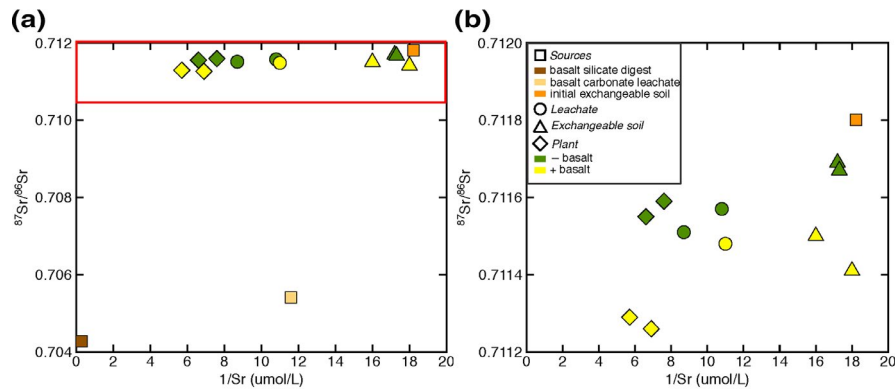


FIGURE 4 Shifts in the strontium isotope composition of the major pools in the mesocosms. (a) Plot shows the $^{87}\text{Sr}/^{86}\text{Sr}$ ratios versus $1/\text{Sr}$ ratios for Sr sources as well as cation reservoirs (i.e. leachate, exchangeable soil and *Sorghum* shoots) in treatment (+basalt) and control (-basalt) soil columns. Red box indicates area expanded in (b). It is likely that $1/\text{Sr}$ ratios in plant, leachate, and exchangeable soil reservoirs do not conservatively trace source mixing in the column due to uptake of Sr by *Sorghum*

that is inaccessible to reacting pore fluids (Brantley & Mellott, 2000) leading to underestimation of surface area-normalized weathering rates. We calculated the apparent RSA using our RTM, constrained by the elemental budgets (Table 2). The RSA value was obtained by optimization, as described above, where the RTM input files were updated with new RSA values. Model goodness-of-fit was evaluated using the root-mean-square difference between Mg release by basalt dissolution and the experimentally determined mass transfer of Mg into the plant, leachate and soil exchange pools in samples collected after 120 days (Table 2). Based on this approach, apparent RSA in our RTM was $7.35 \text{ m}^2/\text{g}$, essentially the same as the BET surface area. Our RTM does not capture repeated evapotranspiration-driven wetting and drying cycles experienced in the soil columns, the formation of preferential flow paths or possible precipitation of secondary minerals occluding dissolving surfaces, as seen in other mesocosm ERW experiments (Amann et al., 2018; Zhang et al., 2018). With constant moisture and drainage, our RTM is comparable to batch reactor experiments where particle surfaces are fully wetted and exposed continually to the fluid. Nevertheless, our modelled leachate Si is slightly underestimated compared to observations, and our Si release rates ($10^{-13} \text{ mol m}^{-2} \text{ s}^{-1}$, Table 2) are lower than those reported for fluid batch reactors with milled basalt particles in the absence of soil and plants ($1.38 \times 10^{-11} \text{ mol Si m}^{-2} \text{ s}^{-1}$ to $7.0 \times 10^{-10} \text{ mol Si m}^{-2} \text{ s}^{-1}$; at 25°C ; Navarre-Sitchler & Brantley, 2007).

3.5 | Strontium isotope evidence for basalt dissolution

Radiogenic Sr isotopes help determine the relative contribution of Sr from cation sources (soil and basalt) to soil column cation reservoirs (plant, soil exchangeable cation sites and leachate). The initial (pretreatment) exchangeable soil $^{87}\text{Sr}/^{86}\text{Sr}$ ratio was the highest of the sample set (0.71180) while the basalt silicate digest and carbonate leachate $^{87}\text{Sr}/^{86}\text{Sr}$ ratios were the lowest of the sample set (0.70428 and 0.70541, respectively). Irrigation water had a Sr

concentration below the detection limit of the ICP-OES and so is assumed to have negligibly contributed to the Sr isotope budget of the soil columns. Urea ($\text{CH}_4\text{N}_2\text{O}$) is assumed to have a negligible Sr component.

Control plant, exchangeable soil and leachate $^{87}\text{Sr}/^{86}\text{Sr}$ ratios were lower than the initial (pretreatment) exchangeable soil $^{87}\text{Sr}/^{86}\text{Sr}$ ratio, suggesting preferential weathering of soil minerals with relatively lower $^{87}\text{Sr}/^{86}\text{Sr}$ ratios throughout the experiment (Figure 4). Treatment (+basalt) plant, exchangeable soil, and leachate $^{87}\text{Sr}/^{86}\text{Sr}$ ratios were lower than the $^{87}\text{Sr}/^{86}\text{Sr}$ ratios of the corresponding reservoirs in the control (-basalt) soil columns and closer to the basalt source (Figure 4). This provides clear evidence for basalt dissolution and its contribution to the cation reservoirs in the treatment soil columns.

Based on the two-component isotope-mixing model (Equation 1), we calculate that approximately 4.1%, 3.0% and 0.9% of Sr in plants, exchangeable soil and leachate, respectively, originate from basalt weathering. These values represent lower limits and marginally increase (4.9%, 3.6% and 1.1%, respectively) if the basalt-derived Sr is assumed to originate from carbonate weathering, and the basalt carbonate leachate $^{87}\text{Sr}/^{86}\text{Sr}$ ratio is implemented in the calculation instead of the basalt silicate digest ratio. These results suggest that dissolved Ca is predominantly retained in the soil column or transferred to plants, with little Ca mobilized into leachate. We note, however, that the transfer of basalt-derived Sr into pedogenic carbonate was not examined but this is likely to be small given no statistically significant change in TIC between the control and treatment columns (Section 3.7).

3.6 | Mycorrhizal fungal grain interactions

Root-associating mycorrhizal fungi are implicated in field trials (Quirk et al., 2012) and experiments (Quirk, Andrews, Leake, Banwart, & Beerling, 2014) in accelerating physical and chemical rates of mineral grain dissolution processes. Consequently, we examined interactions between fungi and basalt grains in the root-excluding nylon

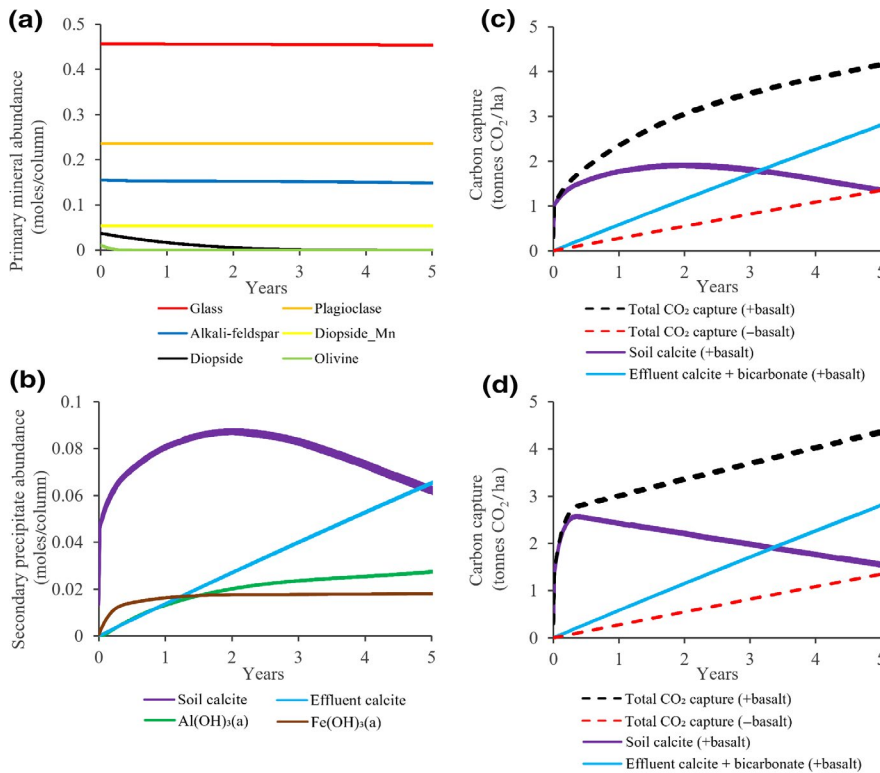


FIGURE 5 Reactive transport modelling of basalt mineral dissolution and carbon capture. Simulated changes in (a) dissolution of individual basaltic mineral components (as moles column⁻¹), (b) secondary mineral or precipitate formation, (c) cumulative CO₂ sequestration with coarse-grained basalt (p80 = 1,250 μm, i.e. 80% of particles ≤ this diameter) and (d) cumulative CO₂ sequestration with a 10-fold finer-grained basalt (p80 = 125 μm)

TABLE 3 Estimated CO₂ sequestration rates from planted mesocosm enhanced rock weathering studies

	Rock material	Rock loading (t rock/ha)	Sequestration period (years)	CO ₂ sequestered (t CO ₂ /ha)	CO ₂ efficiency (t CO ₂ /t rock)	RCO ₂ theoretical maximum ^a
ten Berge et al. (2012)	Olivine	1.63	0.62	0.29 ^b	17.8%	0.91 (19.5%)
	Olivine	204	0.62	2.69 ^b	1.3%	0.91 (1.5%)
Amann et al. (2018)	Dunite	220	1	0.023 ^c	0.01%	0.84 (0.01%)
	Dunite	220	1	0.049 ^c	0.02%	0.84 (0.03%)
Dietzen et al. (2018)	Olivine	10	0.25	3.13 ^d	31.3%	0.69 (45.2%)
	Olivine	50	0.25	4.16 ^d	8.3%	0.69 (12.0%)
Haque et al. (2019)	Wollas-tonite	221	0.15	39.3 ^e	17.8%	0.51 (34.6%)
This study	Basalt	100	1	2.36 ^f	2.4%	0.14 (17.0%)
This study	Basalt	100	1	3.01 ^g	3.0%	0.14 (21.7%)

^aWhere RCO₂ is the ratio of CO₂ removed per mass of rock weathered, calculated from reported MgO and CaO values and RCO₂ equation in Renforth (2012), and the percentage value in parentheses is the fraction of the RCO₂ value attained by the mesocosm trials.

^bCalculated from mass of Mg in plant and soil exchangeable pools.

^cCalculated from mass of Mg in leachate.

^dCalculated from mass of Mg in soil exchangeable pool.

^eCalculated from soil inorganic carbon, alkalinity and thermogravimetric analysis.

^fModelled with particle p80 = 1,280 μm.

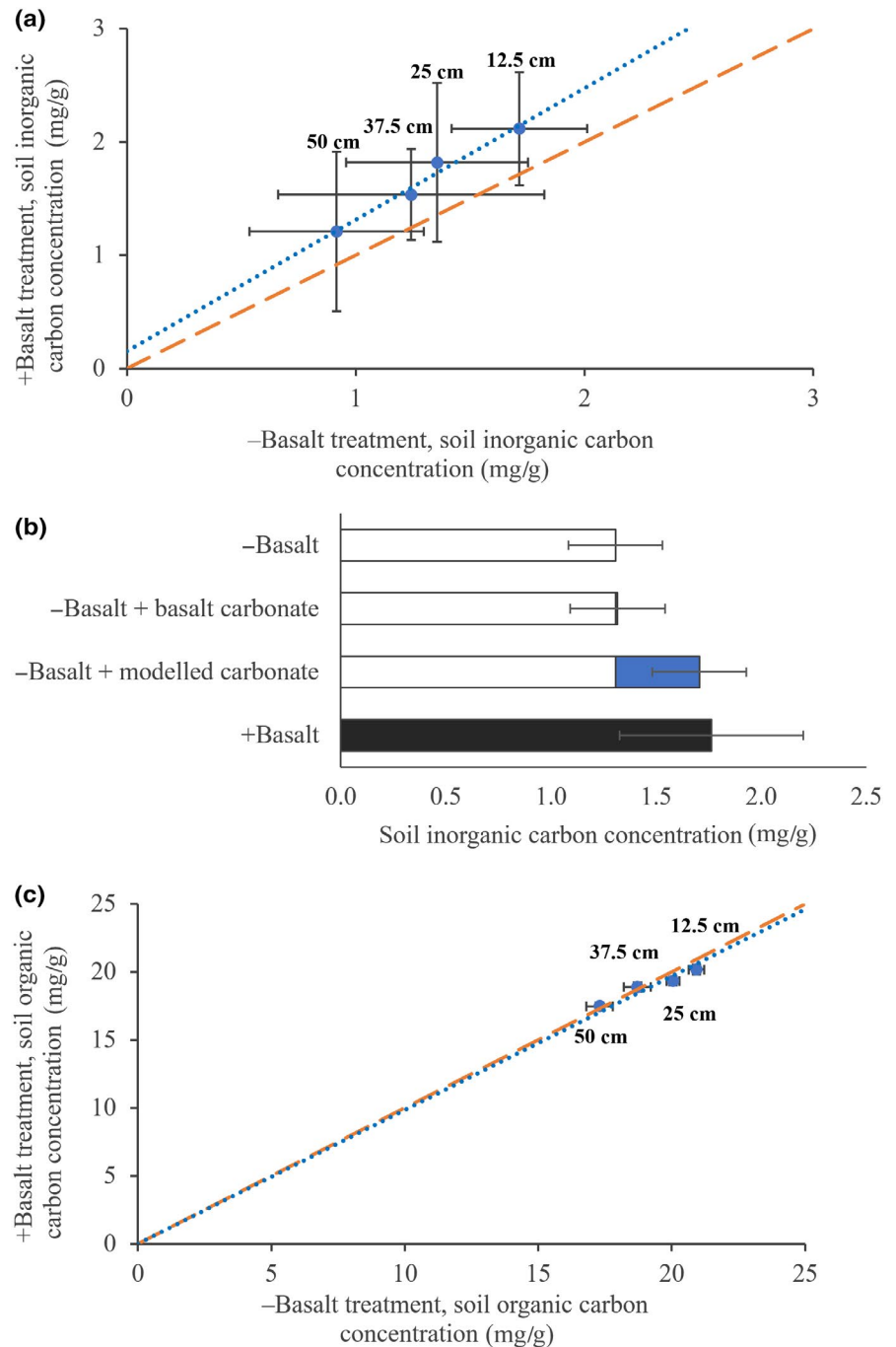
^gModelled with particle p80 = 128 μm.

mesh bags filled with basalt particles in the *Sorghum* root zone (top 15 cm).

Retrieval of rock grains after 120 days indicated extensive colonization by fungi (2.0 ± 0.1 m hyphae/g rock) similar to that reported for crushed basalt-filled mesh-bags buried in soils beneath established (10–30 m high) trees with mycorrhizal fungal partners (Quirk et al.,

2012). Fungal hyphae proliferated throughout grains in the basalt bags, often connecting multiple grains (Figure S7). Hyphae were unpigmented, lacked septa and possessed angular projections (Figure S8), typical characteristics of AM fungi which supply plant roots with nutrients and contribute to bioweathering (Burghel et al., 2015, 2018; Quirk et al., 2012, 2014). DNA extracted from mesh-bags on

FIGURE 6 Measured and modelled soil carbon changes in response to basalt treatment. (a) Comparison of measured total inorganic carbon (TIC) in soils with and without basalt at four depths, normalized to TIC starting concentrations, after 120 days (one-way MANOVA, $p > .05$). Dashed orange line is the 1:1 line. (b) Comparison of observed soil TIC in the postexperimental control (-basalt bar) and basalt-treated (+basalt bar) columns (mean \pm SE for all depths). Also shown is the reactive transport model predicted TIC increase due to result of basalt weathering (-basalt + modelled carbonate stacked bar), which compares favourably with observations (i.e. solid bar), and the very small increase accounted for by native basalt-carbonate dissolution and reprecipitation (-basalt + basalt carbonate). (c) Comparison of measured total soil organic carbon in soils with and without basalt at four depths, normalized to starting concentrations, after 120 days (one-way MANOVA, $p > .05$). Dashed orange line is the 1:1 line. Error bars represent SE



harvesting the plants revealed that up to 45% of the fungal sequences were Glomeromycotina, the phylum-forming AM (Figure S4). This substantial contribution of AM fungi to total fungal DNA likely under-represents their hyphal biomass because not all AM fungal hyphal fragments contain nuclei and they produce fewer spores than other fungal groups identified in the bags and so have a lower DNA:biomass ratio.

Under scanning electron microscopy, weathered grains retrieved from the mesh bags colonized by AM fungi (i.e. postexperiment) had rough, disrupted, surface structures and attached hyphae (Figure S5), whereas unweathered grains (i.e. pretreatment) were characterized by smooth planar surfaces, with

sharper angular geometries, suggesting crystal cleavage surfaces (Figure S6).

3.7 | Modelled basalt dissolution and CO₂ sequestration

Reactive transport model simulations, constrained by observations after 120 days of were run forward in time for 5 years to assess mineral dissolution and carbon capture dynamics beyond the timescale of the experimental trials. Model results suggest that the olivine and diopside basaltic minerals undergo rapid dissolution relative to the

other components (Figure 5a). Simulated basalt dissolution leads to the formation of secondary minerals including calcite (calcium carbonate) and the amorphous phases, $\text{Al}(\text{OH})_3$ and $\text{Fe}(\text{OH})_3$ over time, which act as sinks for the weathered Ca, Al and Fe ions respectively (Figure 5b).

Cumulative total CO_2 sequestration by coarse-grained basalt weathering is simulated to reach $\sim 3 \text{ t CO}_2/\text{ha}$ within 2 years (Figure 5c), and continues to rise towards a maximum of $\sim 4 \text{ t CO}_2/\text{ha}$ after 5 years. Initially, pedogenic carbonate (calcite) formation dominates CO_2 sequestration as the fast-reacting minerals (olivine and diopside) undergo dissolution releasing rapidly divalent cations. Diopside is exhausted after approximately 2 years, and soil-formed calcite begins to dissolve, exiting the systems in the effluent as bicarbonate and reprecipitated calcium carbonate, a storage reservoir that linearly rises over the 5 years of the simulations (Figure 5c). Simulations with a 10-fold smaller particle size distribution result in a faster dissolution of olivine and diopside leading to more rapid CO_2 sequestration via pedogenic carbonate formation (Figure 5d), but with similar cumulative sequestration after 5 years ($4.2 \text{ t CO}_2/\text{ha}$ for the coarse-grained basalt vs. $4.4 \text{ t CO}_2/\text{ha}$ for the 10-fold smaller particles). Amplification of carbon sequestration resulting from the basalt treatment, relative to the 'control columns' was 3.1- and 3.2-fold after 5 years for the two sets of simulations (experiment and small particles respectively). Estimated CO_2 sequestration rates via basalt weathering in our planted mesocosms are comparable with those of prior mesocosm ERW studies in which soils were amended with milled silicates (Table 3). Application rates, types of silicate, irrigation regimes and duration of experiment contribute differences in estimated CO_2 sequestration rates, but lowest rates correspond to studies in which pedogenic carbonate formation has not been estimated (Table 3).

Both sets of RTM simulations support the application of larger particle sizes for Oregon basalt for carbon removal than are typically adopted in ERW numerical studies—or example, 10–20 μm diameter (Köhler et al., 2010; Moosdorf, Renforth, & Hartmann, 2014; Strefler et al., 2018; Taylor et al., 2016). This reduces the energy demands for milling and the associated carbon emissions penalty from the use of fossil fuels (Lefebvre et al., 2019; Moosdorf et al., 2014). In practical terms, carbon removal rates may be lowered by 10%–30% after accounting for CO_2 emissions from logistical operations (mining, grinding, distributing and spreading; Lefebvre et al., 2019; Moosdorf et al., 2014). Nevertheless, our results support ERW as an effective climate change mitigation tool comparable to widely advocated agriculture-based greenhouse gas mitigation measures, including set-aside, grazing land and cropland management options (Paustian et al., 2016).

A TIC budget based on our experimental observations indicates no significant ($p > .05$) change in pedogenic carbonate mineral formation across all depths (Figure 6a) over the 120-day experiment. Statistical comparison of slopes of the fitted regression and the 1:1 line indicated no significant difference ($p > .05$; MANOVA). The modelled change in soil TIC in the postexperiment basalt treated columns is small compared to the background TIC level in the control

columns (Figure 6b). Simulation results (Figure 5b) indicate the duration of our experiment was likely too short to detect a substantial increase soil TIC with basalt treatment (Figure 6). Precipitation of inorganic carbon through pedogenic carbonate formation (Figures 5 and 6) has nevertheless been reported for pot-based trials with wollastonite-amended agricultural soil supporting maize and beans (Haque et al., 2019), and a long-term (7 year) field study (Manning et al., 2013). However, the fate of pedogenic carbonate will depend on seasonal rainfall patterns and land management. Its fate requires assessment in field scale trials under different climatic conditions and farming practices (Zamanian, Pustovoytov, & Kuzyakov, 2016).

We recognize that CO_2 may have been lost from our experimental basalt-treated columns via soil organic matter mineralization, and CO_2 release by respiration in response to increased pH (Malik et al., 2018). However, the agricultural soil in the columns was low in organic matter ($\sim 1\%$), in common with most agricultural soils, and the control and treated soil organic carbon concentrations matched each other after 120 days (Figure 6c). Soil respiration measurements following low (10 t/ha) and high (50 t/ha) applications of finely powdered olivine to an acidic organic-rich podzol soil (pH = 4.9) support this view, with no significant increases in cumulative CO_2 fluxes relative to unamended controls (Dietzen et al., 2018).

4 | CONCLUSIONS

We have shown that amending a slightly acidic clay-loam soil with a high loading of coarse-grained basaltic rock dust substantially increases *Sorghum* yield without P and K fertilizer usage or adverse trace element uptake into the seed, under experimental conditions. Elemental mass budgets indicate that products of basalt dissolution (alkalinity and cations) will not be immediately transported directly to the marine environment via surface waters because of uptake of elements into plant biomass and temporary sequestration onto soil exchangeable sites (e.g. clay and organic matter). Geochemical reactive transport modelling indicates that a single application of basalt might achieve carbon sequestration rates of 2–4 $\text{t CO}_2/\text{ha}$ over 1–5 years. The fates of the newly formed soil carbonates and weathered elements taken up into biomass will depend on land management practices. The long-term fate of these weathering products requires assessment through field trials. Currently, primarily crop grain biomass is removed from fields and the shredded fast-decomposing stover normally returned back to the soils, whereby cations taken up by this unharvested biomass become available to participate in carbon capture.

Our study with a clay-loam soil represents a first step towards supporting the applicability of ERW to European and North American agriculture in which cereals with high silica demand are the most important crops. However, further investigations are warranted at lower rates of basaltic rock dust application to optimize cost effectiveness. If yield improvements follow under field conditions, associated economic gains could offset costs of ERW

deployment. Furthermore, volcanic rock dust is a recognized fertilizer in organic agriculture (Van Straaten, 2006) which, by avoiding superphosphate fertilizers, supports diverse active mycorrhizal fungal networks (Verbruggen et al., 2019) to facilitate mineral dissolution and subsequent CDR (Burghel et al., 2015, 2018; Quirk et al., 2012, 2014). With organic agriculture land area increasing fourfold in 10 years to occupy 57.8 million hectares (in 2018) across 178 countries, our findings highlight new opportunities for upscaling ERW practices in this rapidly expanding sector (Organics International, 2018). Furthermore, it raises the prospect that conventionally managed agricultural land suffering depletion of available silicon pools as a result of intensive cropping, with cereals and straw and stover removal for biofuels and other uses (Haynes, 2017), may also be suitable for ERW.

ACKNOWLEDGEMENTS

We thank Irene Johnson for technical support, Neil Bramall and Scott Young for analytical chemical analyses, Chris Hill for assisting with SEM measurements, Fiona Keay for undertaking the BET measurements, Gren Turner and Jeremy Rushton for assistance with the SEM-EDX analyses and interpretation, and Ian Mounteney for assistance with the XRD sample preparation. Oakbank Game and Conservation, Cambridgeshire, kindly provided Sorghum seeds. We thank Dr Alastair Leake for kindly granting permission to obtain soil from the Game and Wildlife Conservation Trust, Allerton Project farm. M.E.K. and A.L.L. were supported by NERC ACCE DTP studentships. S.J.K. publishes with the permission of the Executive Director, British Geological Survey (UKRI). We gratefully acknowledge funding of this research by the Leverhulme Trust through a Leverhulme Research Centre Award (RC-2015-029).

CONFLICT OF INTEREST

The authors declare that they have no conflict of interest.

AUTHOR CONTRIBUTION

M.E.K., P.W.W., B.S., M.E.H., J.R.L. and D.J.B. designed the study. M.E.K. undertook the experiments, soil and plant measurements and data analysis. P.W.W., L.L.T. and M.E.K. undertook the reactive transport modelling. A.L.L. and S.J.K. undertook basalt geochemistry analyses with B.S. M.G.A. undertook and interpreted strontium isotope geochemistry. R.H.J., C.R.P. and S.A.B. contributed geochemical interpretation. S.E.H. contributed to silicon analyses and interpretation. T.E.A.C. undertook molecular identification and analyses of mycorrhizal fungi. D.J.B., S.A.B. and M.E.K. undertook the writing up with specific contributions and suggestions for references from all other authors.

DATA AVAILABILITY STATEMENT

Raw datasets are included in the Supporting Information tables and the PHREEQ-C code used to interpret the geochemical data and model CO₂ capture is listed in Appendix S1. Additional datasets are available on request from M.E.K.

ORCID

Mike E. Kelland  <https://orcid.org/0000-0002-4901-517X>
 Peter W. Wade  <https://orcid.org/0000-0002-6197-7769>
 Amy L. Lewis  <https://orcid.org/0000-0002-4381-9249>
 Lyla L. Taylor  <https://orcid.org/0000-0002-3406-7452>
 Binoy Sarkar  <https://orcid.org/0000-0002-4196-1225>
 T. E. Anne Cotton  <https://orcid.org/0000-0003-1501-6219>
 Simon J. Kemp  <https://orcid.org/0000-0002-4604-0927>
 Rachael H. James  <https://orcid.org/0000-0001-7402-2315>
 Christopher R. Pearce  <https://orcid.org/0000-0002-4382-2341>
 Sue E. Hartley  <https://orcid.org/0000-0002-5117-687X>
 Mark E. Hodson  <https://orcid.org/0000-0002-8166-1526>
 Jonathan R. Leake  <https://orcid.org/0000-0001-8364-7616>
 Steven A. Banwart  <https://orcid.org/0000-0001-7223-6678>
 David J. Beerling  <https://orcid.org/0000-0003-1869-4314>

REFERENCES

- Amann, T., & Hartmann, J. (2019). Ideas and perspectives: Synergies from co-deployment of negative emission technologies. *Biogeosciences*, 16, 2949–2960. <https://doi.org/10.5194/bg-16-2949-2019>
- Amann, T., Hartmann, J., Struyf, E., de Oliveira Garcia, W., Fischer, E. K., Janssens, I., ... Schoelynck, J. (2018). Enhanced weathering and related element fluxes – A cropland mesocosm approach. *Biogeosciences*, 17, 103–119. <https://doi.org/10.5194/bg-17-103-2020>
- Anda, M., Shamshuddin, J., & Fauziah, C. I. (2013). Increasing negative charge and nutrient contents of a highly weathered soil using basalt and rice husk to promote cocoa growth under field conditions. *Soil and Tillage Research*, 132, 1–11. <https://doi.org/10.1016/j.still.2013.04.005>
- Anda, M., Shamshuddin, J., & Fauziah, C. I. (2015). Improving chemical properties of a highly weathered soil using finely ground basalt rocks. *Catena*, 124, 147–161. <https://doi.org/10.1016/j.catena.2014.09.012>
- Andrews, M. G., Jacobson, A. D., Lehn, G. O., Horton, T. W., & Craw, D. (2016). Radiogenic and stable Sr isotope ratios (⁸⁷Sr/⁸⁶Sr, δ⁸⁸/⁸⁶Sr) as tracers of riverine cation sources and biogeochemical cycling in the Milford Sound region of Fiordland, New Zealand. *Geochimica et Cosmochimica Acta*, 173, 284–303. <https://doi.org/10.1016/j.gca.2015.10.005>
- Appelo, C. A. J., & Postma, D. (2005). *Geochemistry, groundwater and pollution* (2nd ed.). London, UK: CRC Press, Taylor & Francis Group.
- Aradóttir, E. S. P., Sonnenthal, E. L., & Jónsson, H. (2012). Development and evaluation of a thermodynamic dataset for phases of interest in CO₂ mineral sequestration in basaltic rocks. *Chemical Geology*, 304–305, 26–38. <https://doi.org/10.1016/j.chemgeo.2012.01.031>
- Artyszak, A. (2018). Effect of silicon fertilization on crop yield quantity and quality—A literature review in Europe. *Plants*, 7(3), 54. <https://doi.org/10.3390/plants7030054>
- Beerling, D. J., Leake, J. R., Long, S. P., Scholes, J. D., Ton, J., Nelson, P. N., ... Hansen, J. (2018). Farming with crops and rocks to address global climate, food and soil security. *Nature Plants*, 4(3), 138–147. <https://doi.org/10.1038/s41477-018-0108-y>
- Blanc, P., Lassin, A., Piantone, P., Azaroual, M., Jacquemet, N., Fabbri, A., & Gaucher, E. C. (2012). Thermoddem: A geochemical database focused on low temperature water/rock interactions and waste materials. *Applied Geochemistry*, 27(10), 2107–2116. <https://doi.org/10.1016/j.apgeochem.2012.06.002>
- Brantley, S. L., & Mellott, N. P. (2000). Surface area and porosity of primary silicate minerals. *American Mineralogist*, 85(11–12), 1767–1783. <https://doi.org/10.2138/am-2000-11-1220>
- Brunauer, S., Emmett, P. H., & Teller, E. (1938). Adsorption of gases in multimolecular layers. *Journal of the American Chemical Society*, 60(2), 309–319. <https://doi.org/10.1021/ja01269a023>

- Burghelca, C. I., Dontsova, K., Zaharescu, D. G., Maier, R. M., Huxman, T., Amistadi, M. K., ... Chorover, J. (2018). Trace element mobilization during incipient bioweathering of four rock types. *Geochimica et Cosmochimica Acta*, 234, 98–114. <https://doi.org/10.1016/j.gca.2018.05.011>
- Burghelca, C. I., Zaharescu, D. G., Dontsova, K., Maier, R., Huxman, T., & Chorover, J. (2015). Mineral nutrient mobilization by plants from rock: Influence of rock type and arbuscular mycorrhiza. *Biogeochemistry*, 124(1), 187–203. <https://doi.org/10.1007/s10533-015-0092-5>
- Caporaso, J. G., Kuczynski, J., Stombaugh, J., Bittinger, K., Bushman, F. D., Costello, E. K., ... Knight, R. (2010). QIIME allows analysis of high-throughput community sequencing data. *Nature Methods*, 7(5), 335–336. <https://doi.org/10.1038/nmeth.f.303>
- Chapman, H. D. (1965). Cation exchange capacity. In C. A. Black (Ed.), *Methods of soil analysis* (pp. 891–901). Madison, WI: American Society of Agronomy.
- Crooks, R., & Prentice, P. (2017). Extensive investigation into field based responses to a silica fertiliser. *Silicon*, 9(2), 301–304. <https://doi.org/10.1007/s12633-015-9379-3>
- Cuong, T. X., Ullah, H., Datta, A., & Hanh, T. C. (2017). Effects of silicon-based fertilizer on growth, yield and nutrient uptake of rice in tropical zone of Vietnam. *Rice Science*, 24(5), 283–290. <https://doi.org/10.1016/j.rsci.2017.06.002>
- Das, S., Kim, G. W., Hwang, H. Y., Verma, P. P., & Kim, P. J. (2019). Cropping with slag to address soil, environment, and food security. *Frontiers in Microbiology*, 10(1320). <https://doi.org/10.3389/fmicb.2019.01320>
- Daval, D., Sissmann, O., Menguy, N., Saldi, G. D., Guyot, F., Martinez, I., ... Hellmann, R. (2011). Influence of amorphous silica layer formation on the dissolution rate of olivine at 90°C and elevated pCO₂. *Chemical Geology*, 284(1–2), 193–209. <https://doi.org/10.1016/j.chemgeo.2011.02.021>
- de Villiers, O. D. (1961). Soil rejuvenation with crushed basalt in Mauritius. Part I – Consistent results of world-wide interest. *International Sugar Journal*, 63, 363–364.
- Debona, D., Rodrigues, F. A., & Datnoff, L. E. (2017). Silicon's role in abiotic and biotic plant stresses. *Annual Review of Phytopathology*, 55(1), 85–107. <https://doi.org/10.1146/annurev-phyto-080516-035312>
- Dietzen, C., Harrison, R., & Michelsen-Correa, S. (2018). Effectiveness of enhanced mineral weathering as a carbon sequestration tool and alternative to agricultural lime: An incubation experiment. *International Journal of Greenhouse Gas Control*, 74, 251–258. <https://doi.org/10.1016/j.ijggc.2018.05.007>
- EASAC. (2018). *Negative emission technologies: What role in meeting Paris Agreement targets?* Halle, Germany: European Academies Science Advisory Council.
- Edgar, R. C. (2010). Search and clustering orders of magnitude faster than BLAST. *Bioinformatics*, 26(19), 2460–2461. <https://doi.org/10.1093/bioinformatics/btq461>
- Edgar, R. C., Haas, B. J., Clemente, J. C., Quince, C., & Knight, R. (2011). UCHIME improves sensitivity and speed of chimera detection. *Bioinformatics*, 27(16), 2194–2200. <https://doi.org/10.1093/bioinformatics/btr381>
- Edwards, D. P., Lim, F., James, R. H., Pearce, C. R., Scholes, J., Freckleton, R. P., & Beerling, D. J. (2017). Climate change mitigation: Potential benefits and pitfalls of enhanced rock weathering in tropical agriculture. *Biology Letters*, 13, 20160715. <https://doi.org/10.1098/rsbl.2016.0715>
- Flaathen, T. K., Gislason, S. R., & Oelkers, E. H. (2010). The effect of aqueous sulphate on basaltic glass dissolution rates. *Chemical Geology*, 277(3–4), 345–354. <https://doi.org/10.1016/j.chemgeo.2010.08.018>
- Fortner, S. K., Lyons, W. B., Carey, A. E., Shipitalo, M. J., Welch, S. A., & Welch, K. A. (2012). Silicate weathering and CO₂ consumption within agricultural landscapes, the Ohio-Tennessee River Basin, USA. *Biogeosciences*, 9(3), 941–955. <https://doi.org/10.5194/bg-9-941-2012>
- Gillman, G. P. (1980). The effect of crushed basalt scoria on the cation exchange properties of a highly weathered soil. *Soil Science Society of America Journal*, 44(3), 465–468. <https://doi.org/10.2136/sssaj1980.03615995004400030005x>
- Gislason, S. R., & Oelkers, E. H. (2003). Mechanism, rates, and consequences of basaltic glass dissolution: II. An experimental study of the dissolution rates of basaltic glass as a function of pH and temperature. *Geochimica et Cosmochimica Acta*, 67(20), 3817–3832. [https://doi.org/10.1016/S0016-7037\(03\)00176-5](https://doi.org/10.1016/S0016-7037(03)00176-5)
- Guntzer, F., Keller, C., & Meunier, J. D. (2012). Benefits of plant silicon for crops: A review. *Agronomy for Sustainable Development*, 32(1), 201–213. <https://doi.org/10.1007/s13593-011-0039-8>
- Haque, F., Santos, R. M., Dutta, A., Thimmanagari, M., & Chiang, Y. W. (2019). Co-benefits of wollastonite weathering in agriculture: CO₂ sequestration and promoted plant growth. *ACS Omega*, 4(1), 1425–1433. <https://doi.org/10.1021/acsomega.8b02477>
- Hartmann, J., West, A. J., Renforth, P., Köhler, P., De La Rocha, C. L., Wolf-Gladrow, D. A., ... Scheffran, J. (2013). Enhanced chemical weathering as a geoengineering strategy to reduce atmospheric carbon dioxide, supply nutrients, and mitigate ocean acidification. *Reviews of Geophysics*, 51(2), 113–149. <https://doi.org/10.1002/rog.20004>
- Haynes, R. J. (2017). Significance and role of Si in crop production. *Advances in Agronomy*, 146, 83–166. <https://doi.org/10.1016/bs.agron.2017.06.001>
- Hellenbrandt, M. (2004). The inorganic crystal structure database (ICSD) – Present and future. *Crystallography Reviews*, 10(1), 17–22. <https://doi.org/10.1080/08893110410001664882>
- Hindumathi, A., & Reddy, B. N. (2011). Dependency of sorghum on arbuscular mycorrhizal colonization for growth and development. *Journal of Mycology and Plant Pathology*, 41(4), 537–542.
- Ihrmark, K., Bodeker, I. T. M., Cruz-Martinez, K., Friberg, H., Kubartova, A., Schenck, J., ... Lindahl, B. D. (2012). New primers to amplify the fungal ITS2 region – Evaluation by 454-sequencing of artificial and natural communities. *FEMS Microbiology Ecology*, 82(3), 666–677. <https://doi.org/10.1111/j.1574-6941.2012.01437.x>
- Kantola, I. B., Masters, M. D., Beerling, D. J., Long, S. P., & DeLucia, E. H. (2017). Potential of global croplands and bioenergy crops for climate change mitigation through deployment for enhanced weathering. *Biology Letters*, 13, 20160714. <https://doi.org/10.1098/rsbl.2016.0714>
- Kemp, S. J., Smith, F. W., Wagner, D., Mounteney, I., Bell, C. P., Milne, C. J., ... Pottas, T. L. (2016). An improved approach to characterize potash-bearing evaporite deposits, evidenced in North Yorkshire, United Kingdom. *Economic Geology*, 111(3), 719–742. <https://doi.org/10.2113/econgeo.111.3.719>
- Kirchner, J. (2001). Data Analysis Toolkit #5: Uncertainty Analysis and Error Propagation. UC California Berkeley Seismological Laboratory. Retrieved from http://seismo.berkeley.edu/~kirchner/eps_120/Toolkits/Toolkit_05.pdf
- Köhler, P., Hartmann, J., & Wolf-Gladrow, D. A. (2010). Geoengineering potential of artificially enhanced silicate weathering of olivine. *Proceedings of the National Academy of Sciences of the United States of America*, 107(47), 20228–20233. <https://doi.org/10.1073/pnas.1000545107>
- Korchagin, J., Caner, L., & Bortoluzzi, E. C. (2019). Variability of amethyst mining waste: A mineralogical and geochemical approach to evaluate the potential use in agriculture. *Journal of Cleaner Production*, 210, 749–758. <https://doi.org/10.1016/j.jclepro.2018.11.039>
- Lefebvre, D., Goglio, P., Williams, A., Manning, D. A. C., de Azevedo, A. C., Bergmann, M., ... Smith, P. (2019). Assessing the potential of soil carbonation and enhanced weathering through Life Cycle Assessment: A case study for Sao Paulo State, Brazil. *Journal of Cleaner Production*, 233, 468–481. <https://doi.org/10.1016/j.jclepro.2019.06.099>

- Li, Z., Song, Z., Yan, Z., Hao, Q., Song, A., Liu, L., ... Liang, Y. (2018). Silicon enhancement of estimated plant biomass carbon accumulation under abiotic and biotic stresses. A meta-analysis. *Agronomy for Sustainable Development*, 38(26). <https://doi.org/10.1007/s13593-018-0496-4>
- Liu, J., Zhu, J., Zhang, P., Han, L., Reynolds, O. L., Zeng, R., ... Gurr, G. M. (2017). Silicon supplementation alters the composition of herbivore induced plant volatiles and enhances attraction of parasitoids to infested rice plants. *Frontiers in Plant Science*, 8, 1–8. <https://doi.org/10.3389/fpls.2017.01265>
- Ma, J. F. (2004). Role of silicon in enhancing the resistance of plants to biotic and abiotic stresses. *Soil Science and Plant Nutrition*, 50(1), 11–18. <https://doi.org/10.1080/00380768.2004.10408447>
- Ma, J. F., & Yamaji, N. (2006). Silicon uptake and accumulation in higher plants. *Trends in Plant Science*, 11(8), 392–397. <https://doi.org/10.1016/j.tplants.2006.06.007>
- Majaneva, M., Hyttiäinen, K., Varvio, S. L., Nagai, S., & Blomster, J. (2015). Bioinformatic amplicon read processing strategies strongly affect eukaryotic diversity and the taxonomic composition of communities. *PLoS ONE*, 10(6), 1–18. <https://doi.org/10.1371/journal.pone.0130035>
- Malik, A. A., Puissant, J., Buckeridge, K. M., Goodall, T., Jehmlich, N., Chowdhury, S., ... Griffiths, R. I. (2018). Land use driven change in soil pH affects microbial carbon cycling processes. *Nature Communications*, 9(1), 1–10. <https://doi.org/10.1038/s41467-018-05980-1>
- Manning, D. A. C., Renforth, P., Lopez-Capel, E., Robertson, S., & Ghazireh, N. (2013). Carbonate precipitation in artificial soils produced from basaltic quarry fines and composts: An opportunity for passive carbon sequestration. *International Journal of Greenhouse Gas Control*, 17, 309–317. <https://doi.org/10.1016/j.ijggc.2013.05.012>
- Meena, V. D., Dotaniya, M. L., Coumar, V., Rajendiran, S., Kundu, A. S., & Subba Rao, A. (2014). A case for silicon fertilization to improve crop yields in tropical soils. *Proceedings of the National Academy of Sciences India Section B - Biological Sciences*, 84(3), 505–518. <https://doi.org/10.1007/s40011-013-0270-y>
- Meharg, C., & Meharg, A. A. (2015). Silicon, the silver bullet for mitigating biotic and abiotic stress, and improving grain quality, in rice? *Environmental and Experimental Botany*, 120, 8–17. <https://doi.org/10.1016/j.envexpbot.2015.07.001>
- Moosdorf, N., Renforth, P., & Hartmann, J. (2014). Carbon dioxide efficiency of terrestrial enhanced weathering. *Environmental Science & Technology*, 48, 4809–4816. <https://doi.org/10.1021/es4052022>
- Nan, W., Yue, S., Li, S., Huang, H., & Shen, Y. (2016). The factors related to carbon dioxide effluxes and production in the soil profiles of rain-fed maize fields. *Agriculture, Ecosystems and Environment*, 216, 177–187. <https://doi.org/10.1016/j.agee.2015.09.032>
- Navarre-Sitchler, A., & Brantley, S. (2007). Basalt weathering across scales. *Earth and Planetary Science Letters*, 261(1–2), 321–334. <https://doi.org/10.1016/j.epsl.2007.07.010>
- Nesbitt, H. W., & Young, G. (1982). Early Proterozoic climates and plate motions inferred from major element chemistry of lutites. *Nature*, 299, 715–717. <https://doi.org/10.1038/299715a0>
- Nilsson, R. H., Larsson, K. H., Taylor, A. F. S., Bengtsson-Palme, J., Jeppesen, T. S., Schigel, D., ... Abarenkov, K. (2019). The UNITE database for molecular identification of fungi: Handling dark taxa and parallel taxonomic classifications. *Nucleic Acids Research*, 47(D1), D259–D264. <https://doi.org/10.1093/nar/gky1022>
- NRC. (2015). *Climate intervention: Carbon dioxide removal and reliable sequestration*. Washington, DC: The National Academies Press.
- Organics International. (2018). *World of organic agriculture. Statistics and emerging trends 2018* (H. Willer & J. Lernoud Eds.; 18th ed.). Bonn, Germany: Research Institute of Organic Agriculture, Organic International.
- Palandri, J. L., & Kharaka, Y. K. (2004). *A compilation of rate parameters of water-mineral interaction kinetics for application to geochemical modeling*. Report No. 2004-1068 (pp. 1–64). Menlo Park, CA: U.S. Geological Survey.
- Parkhurst, D. L., & Apello, T. (2013). *Description of input and examples for PHREEQC version 3—A computer program for speciation, batch-reaction, one-dimensional transport, and inverse geochemical calculations*. US Geological Survey Techniques and Methods, Book 6, Chapter A43 (pp. 1–497). Denver, CO: US Geological Survey.
- Paustian, K., Lehmann, J., Ogle, S., Reay, D., Robertson, G. P., & Smith, P. (2016). Climate-smart soils. *Nature*, 532(7597), 49–57. <https://doi.org/10.1038/nature17174>
- Pétriaccq, P., Williams, A., Cotton, T. E. A., McFarlane, A. E., Rolfe, S. A., & Ton, J. (2017). Metabolite profiling of non-sterile rhizosphere soil. *The Plant Journal*, 92, 147–162. <https://doi.org/10.1111/tpj.13639>
- Potter, P., Ramankutty, N., Bennett, E. M., & Donner, S. D. (2010). Characterizing the spatial patterns of global fertilizer application and manure production. *Earth Interactions*, 14(2), 1–22. <https://doi.org/10.1175/2009EI288.1>
- Quirk, J., Andrews, M. Y., Leake, J. R., Banwart, S. A., & Beerling, D. J. (2014). Ectomycorrhizal fungi and past high CO₂ atmospheres enhance mineral weathering through increased below-ground carbon-energy fluxes. *Biology Letters*, 10(7), 20140375. <https://doi.org/10.1098/rsbl.2014.0375>
- Quirk, J., Beerling, D. J., Banwart, S. A., Kakonyi, G., Romero-Gonzalez, M. E., & Leake, J. R. (2012). Evolution of trees and mycorrhizal fungi intensifies silicate mineral weathering. *Biology Letters*, 8(6), 1006–1011. <https://doi.org/10.1098/rsbl.2012.0503>
- Reidinger, S., Ramsey, M. H., & Hartley, S. E. (2012). Rapid and accurate analyses of silicon and phosphorus in plants using a portable X-ray fluorescence spectrometer Methods Rapid and accurate analyses of silicon and phosphorus in plants using a portable X-ray fluorescence spectrometer. *New Phytologist*, 195, 699–706. <https://doi.org/10.1111/j.1469-8137.2012.04179.x>
- Renforth, P. (2012). The potential of enhanced weathering in the UK. *International Journal of Greenhouse Gas Control*, 10, 229–243. <https://doi.org/10.1016/j.ijggc.2012.06.011>
- Renforth, P., & Henderson, G. (2017). Assessing ocean alkalinity for carbon sequestration. *Reviews of Geophysics*, 55(3), 636–674. <https://doi.org/10.1002/2016RG000533>
- Renforth, P., Pogge von Strandmann, P. A. E., & Henderson, G. M. (2015). The dissolution of olivine added to soil: Implications for enhanced weathering. *Applied Geochemistry*, 61, 109–118. <https://doi.org/10.1016/j.apgeochem.2015.05.016>
- Rimstidt, J. D. (2014). *Geochemical rate models: An introduction to geochemical kinetics*. New York, NY: Cambridge University Press.
- Smith, G. A., & Hayman, G. A. (1987). *Geologic map of the Eagle Butte and Gateway quadrangles, Jefferson and Wasco Counties, Oregon*. 1:24,000. *Geological Map Series* 43.
- Smith, P., Adams, J., Beerling, D. J., Beringer, T., Calvin, K. V., Fuss, S., ... Keesstra, S. (2019). Impacts of land-based greenhouse gas removal options on ecosystem services and the United Nations sustainable development goals. *Annual Review of Environment and Resources*, 44(1), 1–32. <https://doi.org/10.1146/annurev-environ-101718-033129>
- Strefler, J., Amann, T., Bauer, N., Kriegler, E., & Hartmann, J. (2018). Potential and costs of carbon dioxide removal by enhanced weathering of rocks. *Environmental Research Letters*, 13, 034010. <https://doi.org/10.1088/1748-9326/aaa9c4>
- Taylor, L. L., Quirk, J., Thorley, R. M. S., Kharecha, P. A., Hansen, J., Ridgwell, A., ... Beerling, D. J. (2016). Enhanced weathering strategies for stabilizing climate and averting ocean acidification. *Nature Climate Change*, 6(4), 402–406. <https://doi.org/10.1038/nclimate2882>
- ten Berge, H. F. M., van der Meer, H. G., Steenhuizen, J. W., Goedhart, P. W., Knops, P., & Verhagen, J. (2012). Olivine weathering in soil, and its effects on growth and nutrient uptake in ryegrass (*Lolium perenne* L.): A pot experiment. *PLoS ONE*, 7(8), e42098. <https://doi.org/10.1371/journal.pone.0042098>
- Tippling, E. (1998). Humic ion-binding model VI: An improved description of the interactions of protons and metal ions with humic substances.

- Aquatic Geochemistry*, 4(1), 3–48. <https://doi.org/10.1023/A:1009627214459>
- Tipping, E., & Hurley, M. A. (1992). A unifying model of cation binding by humic substances. *Geochimica et Cosmochimica Acta*, 56(10), 3627–3641. [https://doi.org/10.1016/0016-7037\(92\)90158-F](https://doi.org/10.1016/0016-7037(92)90158-F)
- Tubana, B. S., Babu, T., & Datnoff, L. E. (2016). A review of silicon in soils and plants and its role in us agriculture: History and future perspectives. *Soil Science*, 181(9–10), 393–411. <https://doi.org/10.1097/SS.0000000000000179>
- Turhollow, A. F., Webb, E. G., & Downing, M. E. (2010). *Review of sorghum production practices: Applications for bioenergy*. Oak Ridge, TN: U.S. Department of Energy.
- UNEP. (2018). *The emissions gap report 2018*. Nairobi, Kenya: United Nations Environment Programme.
- Van Bockhaven, J., De Vleeschauwer, D., & Höfte, M. (2012). Towards establishing broad-spectrum disease resistance in plants: Silicon leads the way. *Journal of Experimental Botany*, 64(5), 1281–1293. <https://doi.org/10.1093/jxb/ers329>
- Van Straaten, P. (2006). Farming with rocks and minerals: Challenges and opportunities. *Annals of the Brazilian Academy of Sciences*, 78(4), 731–747. <https://doi.org/10.1590/S0001-37652006000400009>
- Verbruggen, E., Röling, W. F. M., Gamper, H. A., Kowalchuk, G. A., Verhoef, H. A., & van der Heijden, M. G. A. (2019). Positive effects of organic farming on below-ground mutualists: Large-scale comparison of mycorrhizal fungal communities in agricultural soils. *New Phytologist*, 186(4), 968–979. <https://doi.org/10.1111/j.1469-8137.2010.03230.x>
- West, T. O., & McBride, A. C. (2005). The contribution of agricultural lime to carbon dioxide emissions in the United States: Dissolution, transport, and net emissions. *Agriculture, Ecosystems and Environment*, 108(2), 145–154. <https://doi.org/10.1016/j.agee.2005.01.002>
- White, T. J., Bruns, T., Lee, S., & Taylor, J. W. (1990). Amplification and direct sequencing of fungal ribosomal RNA genes for phylogenetics. In M. A. Innis, D. H. Gelfand, J. J. Sninsky, & T. J. White (Eds.), *PCR protocols: A guide to methods and applications* (pp. 315–322). New York, NY: Academic Press Inc.
- Zamanian, K., Pustovoytov, K., & Kuzyakov, Y. (2016). Pedogenic carbonates: Forms and formation processes. *Earth-Science Reviews*, 157, 1–17. <https://doi.org/10.1016/j.earscirev.2016.03.003>
- Zhang, G. R., Kang, J. T., Wang, T. X., & Zhu, C. (2018). Review and outlook for agromineral research in agriculture and climate mitigation. *Soil Research*, 56(2), 113–122. <https://doi.org/10.1071/SR17157>

SUPPORTING INFORMATION

Additional supporting information may be found online in the Supporting Information section.

How to cite this article: Kelland ME, Wade PW, Lewis AL, et al. Increased yield and CO₂ sequestration potential with the C₄ cereal *Sorghum bicolor* cultivated in basaltic rock dust-amended agricultural soil. *Glob Change Biol*. 2020;26: 3658–3676. <https://doi.org/10.1111/gcb.15089>